Monthly Notices
of the
ROYAL ASTRONOMICAL SOCIETY

Mon. Not. R. Astron. Soc. **416,** 2981–2996 (2011) doi:10.1111/j.1365-2966.2011.19247.x

A strategy to measure the dark energy equation of state using the H II galaxy Hubble function and X-ray active galactic nuclei clustering: preliminary results

M. Plionis,[1,2⋆] R. Terlevich,[2] S. Basilakos,[3,4] F. Bresolin,[5] E. Terlevich,[2] J. Melnick[6] and R. Chavez[2]

[1]*Institute of Astronomy & Astrophysics, National Observatory of Athens, Palaia Penteli, 152 36 Athens, Greece*
[2]*Instituto Nacional de Astrofísica Optica y Electrónica, AP 51 y 216, 72000 Puebla, Mexico*
[3]*Academy of Athens, Research Center for Astronomy and Applied Mathematics, Soranou Efesiou 4, 11527 Athens, Greece*
[4]*High Energy Physics Group, Dept. ECM, Universitat de Barcelona, Av. Diagonal 647, E-08028 Barcelona, Spain*
[5]*Institute for Astronomy of the University of Hawaii, 2680 Woodlawn Drive, Honolulu, HI 96822, USA*
[6]*European Southern Observatory, Alonso de Cordoba 3107, Santiago, Chile*

Accepted 2011 June 14. Received 2011 June 6; in original form 2011 April 5

ABSTRACT

We explore the possibility of setting stringent constraints to the dark energy equation of state using alternative cosmic tracers like (a) the Hubble relation using H II galaxies, which can be observed at much higher redshifts ($z \lesssim 3.5$) than those currently traced by Type Ia supernovae (SNeIa) samples, and (b) the large-scale structure using the clustering of X-ray selected active galactic nuclei (AGN), which have a redshift distribution peaking at $z \sim 1$.

In this paper we use extensive Monte Carlo simulations to define the optimal strategy for the recovery of the dark energy equation of state using the high-redshift ($z \gtrsim 2$) Hubble relation, but accounting also for the effects of gravitational lensing, which for such high redshifts can significantly affect the derived cosmological constraints. We investigate the size of the sample of high-z H II galaxies needed to provide useful constraints in the dark energy equation of state. Based on a 'figure of merit' analysis, we provide estimates for the number of $2 \lesssim z \lesssim 3.5$ tracers needed to reduce the cosmological solution space, presently provided by the *Constitution* SNIa set, by a desired factor. The analysis is given for any level of rms distance modulus uncertainty and we find that an expected reduction (i.e. by ∼20–40 per cent) of the current level of H II-galaxy-based distance modulus uncertainty does not provide a significant improvement in the derived cosmological constraints. It is much more efficient to increase the number of tracers than to reduce their individual uncertainties.

Finally, we propose a framework to put constraints on the dark energy equation of state by using the joint likelihood of the X-ray AGN clustering and of the Hubble relation cosmological analyses. A preliminary joint analysis using the X-ray AGN clustering of the 2*XMM* survey and the Hubble relation of the *Constitution* SNIa set provide $\Omega_{\rm m} = 0.31 \pm 0.01$ and $w = -1.06 \pm 0.05$. We also find that the joint SNIa–2*XMM* analysis provides significantly more stringent cosmological constraints, increasing the figure of merit by a factor of ∼2, with respect to that of the joint SNIa–baryonic acoustic oscillation analysis.

Key words: galaxies: active – galaxies: starburst – cosmological parameters – dark energy – large-scale structure of Universe – X-rays: galaxies.

1 INTRODUCTION

We live in a very exciting period for our understanding of the cosmos. Over the past decade the accumulation and detailed analyses of high-quality cosmological data [e.g. Type Ia supernovae (SNeIa), cosmic microwave background (CMB) temperature fluctuations, galaxy clustering, high-z clusters of galaxies, etc.] have strongly suggested that we live in a flat and accelerating universe, which contains at least some sort of cold dark matter (CDM) to explain the clustering of extragalactic sources, and an extra component which acts as having a negative pressure, as for example the energy of

⋆E-mail: mplionis@astro.noa.gr

the vacuum [or in a more general setting the so-called dark energy (DE)], to explain the observed accelerated cosmic expansion (e.g. Riess et al. 1998, 2004; Perlmutter et al. 1999; Schuecker et al. 2003; Spergel et al. 2003, 2007; Tonry et al. 2003; Allen et al. 2004; Tegmark et al. 2004; Basilakos & Plionis 2005, 2006, 2009, hereafter BP09; Seljak et al. 2005; Blake et al. 2007; Davis et al. 2007, hereafter D07; Riess et al. 2007; Wood-Vasey et al. 2007; Kowalski et al. 2008; Hicken et al. 2009; Komatsu et al. 2009; Amanullah et al. 2010, etc.).

Because of the absence of a well-motivated fundamental theory, there have been many theoretical speculations regarding the nature of the DE, on whether it is a cosmological constant or a field that provides a time varying equation of state, usually parametrized by

$$p_{\rm Q} = w(z)\rho_{\rm Q}, \tag{1}$$

with $p_{\rm Q}$ and $\rho_{\rm Q}$ the pressure and density of the exotic DE fluid. For a large class of DE models, we have

$$w(z) = w_0 + w_1 f(z), \tag{2}$$

with $w_0 = w(z = 0)$ and $f(z)$ an increasing function of redshift. A particular example of $w(z)$ is its first-order Taylor's expansion around $w(0)$, which provides $f(z) = z/(1 + z)$, i.e. the so-called CPL form of the DE equation of state (Chevallier & Polarski 2001; Linder 2003; see also Peebles & Ratra 2003; Dicus & Repko 2004; Wang & Mukherjee 2006). Of course, it could also be conceived that the equation of state parameter does not evolve cosmologically [quintessence dark energy (QDE) model].

It is clear that one of the most important questions in cosmology and cosmic structure formation is related to the nature of DE (as well as whether it is the sole explanation of the observed accelerated expansion of the Universe) and its interpretation within a fundamental physical theory (e.g. Albrecht et al. 2006; Peacock et al. 2006). To this end, a large number of very expensive experiments are proposed and/or are at various stages of development, viz. the Dark Energy Survey: http://www.darkenergysurvey.org/, the Joint Dark Energy Mission: http://jdem.gsfc.nasa.gov/, the Hobby–Eberly Telescope Dark Energy Experiment: http://www.as.utexas.edu/hetdex/, the Panoramic Survey Telescope and Rapid Response System: http://pan-starrs.ifa.hawaii.edu, Euclid: http://sci.esa.int/euclid/, Wfirst: http://wfirst.gsfc.nasa.gov, etc.

Therefore, the paramount importance of the detection and quantification of DE for our understanding of the cosmos and for fundamental theories implies that the results of the different experiments should not only be scrutinized, but alternative, even higher risk, methods to measure DE should be developed and applied as well. It is within this paradigm that our current work falls. Indeed, we wish to constrain the DE equation of state using, individually and in combination, the Hubble relation and large-scale structure (clustering) methods, but utilizing alternative cosmic tracers for both of these components.

Thus, we will trace the Hubble relation using H II galaxies, which can be observed at higher redshifts than reached by current SNIa surveys to distances where the Hubble relation is more sensitive to the cosmological parameters. The H II galaxies can be used as standard candles (Melnick, Terlevich & Terlevich 2000; Melnick 2003; Siegel et al. 2005; Plionis et al. 2009) due to the correlation between their velocity dispersion, Hβ luminosity and metallicity (Melnick 1978; Terlevich & Melnick 1981; Melnick, Terlevich & Moles 1988). Furthermore, the use of such alternative high-z tracer will enable us to check the SNIa results and lift any doubts that arise from the fact that they are the only tracers of the Hubble relation used to-date [for possible usage of gamma-ray bursts (GRBs) see e.g. Ghirlanda, Ghisellini & Firmani 2006; Basilakos & Perivolaropoulos 2008; Ghirlanda 2009, and references therein].[1]

Additionally, we use X-ray selected active galactic nuclei (AGN) at a median redshift of $\sim$1, which is roughly the peak of their redshift distribution (see Basilakos et al. 2004, 2005; Miyaji et al. 2007), in order to determine their clustering pattern and compare it with that predicted by different cosmological models (see Matsubara 2004).

Although each of the previously discussed components of our project (Hubble relation using H II galaxies and angular/spatial clustering of X-ray AGN) will provide interesting and relatively stringent constraints on the cosmological parameters, especially under our anticipation that we will reduce significantly the corresponding random and systematic errors, it is the combined likelihood of these two type of analyses that enables us to break the known degeneracies between cosmological parameters and determine with great accuracy the DE equation of state (see Basilakos & Plionis 2005, 2006; BP09).

Below we present the basic methodology and expectations of the two components of our method. In Section 2 we present the details of the first component where we develop a Monte Carlo simulation approach designed to ultimately provide a rule of thumb of how many H II galaxies we need to obtain a particular level of the DE equation of state parameter uncertainty. We also develop a method to account for the effects of gravitational lensing, which at such high redshifts are significant. In Section 3 we present the details of the second component, and in Section 4 we present an example of joining the two components to provide cosmological constraints. The conclusions are listed in Section 5.

2 COSMOLOGICAL PARAMETERS FROM THE HUBBLE RELATION

In the matter-dominated epoch, the Hubble relation depends on the cosmological parameters via the following equation:

$$H(z) = H_0 E(z), \tag{3}$$

with

$$E^2(z) = \Omega_{\rm m}(1+z)^3 + \Omega_{\rm k}(1+z)^2 + \Omega_{\rm Q}\exp\left[3\int_0^z \frac{1+w(x)}{1+x}\,{\rm d}x\right], \tag{4}$$

which is simply derived from Friedman's equation. We remind the reader that $\Omega_{\rm m}$, $\Omega_{\rm k}$ and $\Omega_{\rm Q}(\equiv 1 - \Omega_{\rm m} - \Omega_{\rm k})$ are the present fractional contributions to the total cosmic mass-energy density of the matter, the spatial curvature and DE source terms, respectively.

SNeIa are considered standard candles at peak luminosity and therefore they have been used not only to determine the Hubble constant (at relatively low redshifts) but also to trace the curvature

[1] GRBs appear to be anything but standard candles, having a very wide range of isotropic equivalent luminosities and energy outputs. Nevertheless, correlations between various properties of the prompt emission and in some cases also the afterglow emission have been used to determine their distances. A serious problem that hampers a straightforward use of GRBs as cosmological probes is the intrinsic faintness of the nearby events, a fact which introduces a bias towards low (or high) values of GRB observables and therefore the extrapolation of their correlations to low-z events is faced with serious problems. One might also expect a significant evolution of the intrinsic properties of GRBs with redshift (also between intermediate and high redshifts) which can be hard to disentangle from cosmological effects. Finally, even if a reliable scaling relation can be identified and used, the scatter in the resulting luminosity and thus distance modulus is still fairly large.

of the Hubble relation at high redshifts (see Perlmutter et al. 1998, 1999; Riess et al. 1998, 2004; Tonry et al. 2003; Astier et al. 2006; D07; Riess 2007; Wood-Vasey et al. 2007; Kowalski et al. 2008; Hicken et al. 2009; Amanullah et al. 2010; Adak, Bandyopadhyay & Majumdar 2011; Kim 2011; Li et al. 2011; March et al. 2011; Wang, Li & Li 2011). In practice one relates the distance modulus of the SNIa to its luminosity distance, d_L, through which the cosmological parameters enter:

$$\mu = m - M = 5 \log d_L + 25 \tag{5}$$

and

$$d_L = \frac{c(1+z)}{H_0\sqrt{\Omega_k}} \sinh\left[\sqrt{\Omega_k}\int_0^z \frac{dx}{E(x)}\right], \tag{6}$$

which for a flat universe ($\Omega_k = 0$) reduces to

$$d_L = \frac{c(1+z)}{H_0}\int_0^z \frac{dx}{E(x)}. \tag{7}$$

The main result of numerous studies using this procedure is that distant SNeIa's are on average dimmer by ∼0.2 mag than expected in an Einstein–de Sitter model, which translates in them being ∼10 per cent further away than expected.

The amazing consequence of these results is that we live in an accelerating phase of the expansion of the Universe, an assertion that needs to be scrutinized on all possible levels, one of which is to verify the accelerated expansion of the Universe using alternative to SNIa's extragalactic standard candles. Furthermore, the cause and rate of the acceleration is of paramount importance, i.e. the DE equation of state is the next fundamental item to search for and to these directions we hope to contribute with our current project.

2.1 Theoretical expectations

To appreciate the magnitude of the Hubble relation variations due to the different DE equation of states, we plot in Fig. 1 the relative deviations of the distance modulus, $\Delta\mu$, of different DE models from a nominal *standard* ($w = -1$) Λ cosmology (with $\Omega_m = 0.27$ and $\Omega_\Lambda = 0.73$), with the relative deviations defined as

$$\Delta\mu = \mu_\Lambda - \mu_{\rm model}. \tag{8}$$

The parameters of the different models used are shown in Fig. 1. As far as the DE equation of state parameter is concerned, we present the deviations from the *standard* model of two models with a constant w value and of two models with an evolving equation of state parameter, utilizing the form of equation (2). In the left-hand panel of Fig. 1 we present results for selected values of Ω_m, while in the right-hand panel we use the same DE equations of state parameters but for the same value of $\Omega_m (= 0.27)$ (i.e. we avoid the Ω_m–$w(z)$ degeneracy).

Three important observations should be made from Fig. 1.

(i) The relative magnitude deviations between the different DE models are quite small (typically $\lesssim$0.1 mag), which puts severe pressure on the necessary photometric accuracy of the relevant observations.

(ii) The largest relative deviations of the distance moduli occur at redshifts $z \gtrsim 1.5$, quite larger than those currently traced by SNIa samples.

(iii) There are strong degeneracies between the different cosmological models at redshifts $z \lesssim 1$, and in some models even up to much higher redshifts [e.g. between the models with (Ω_m, w_0, w_1) = (0.31, −1, 0) and (0.29, −1, 0.3); see Fig. 1].

Luckily, as discussed already in the Introduction, such degeneracies can be broken by using other cosmological probes [e.g. the clustering of extragalactic sources, the CMB shift parameter, baryonic acoustic oscillation (BAO), etc.]. Indeed, current evidence overwhelmingly show that the total matter content of the universe is within the range: $0.2 \lesssim \Omega_m \lesssim 0.3$, a fact that reduces significantly the degeneracies between the cosmological parameters.

2.2 Gravitational lensing effects on high-z distance moduli

A potentially important systematic effect that could hinder attempts to put stringent cosmological constraints via the Hubble relation, especially when using high-z standard candles (which as we saw are those precisely that differentiate between DE equations of state) is related to gravitational lensing by structures intervening between source and receptor. It is indeed known that the gravitational potential of large-scale structure affects the propagation of light from high-redshift sources and thus also the distance modulus of similarly high-redshift standard candles (e.g. Holz & Wald 1998; Holz & Linder 2005, hereafter HL05; Brouzakis & Tetradis 2008 and references therein). These studies assume a Robertson–Walker background superimposing a locally inhomogeneous universe and take into account both strong and weak lensing effects. The resulting magnification distribution of a single source over different paths is

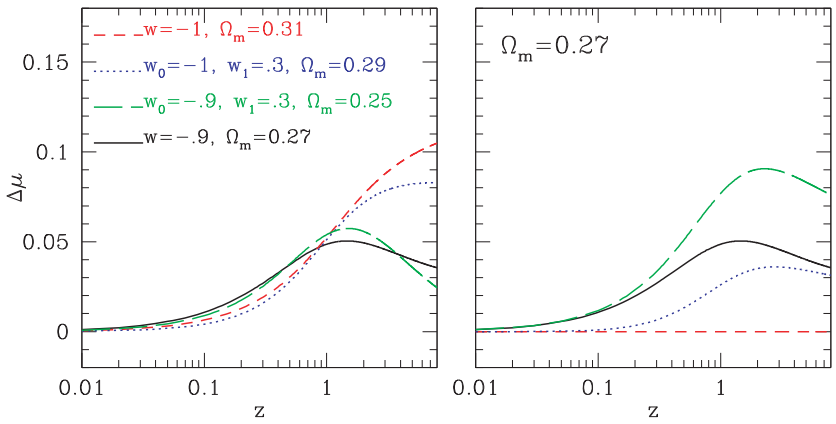

Figure 1. Left-hand panel: the expected distance modulus difference between the DE models shown and the reference Λ model ($w = -1$) with $\Omega_m = 0.27$. Right-hand panel: the expected distance modulus differences once the Ω_m–$w(z)$ degeneracy is broken (imposing the same Ω_m value as in the comparison model).

non-Gaussian and therefore has a non-trivial effect on its distance modulus, especially so for the high-z standard candles.

The main characteristics of the magnification probability density function, $P(\mu_a)$, as derived from a variety of studies based on Monte Carlo analyses and ray-tracing techniques, is that $P(\mu_a)$ resembles a lognormal distribution with zero mean (the mean flux of each source over all possible different paths is conserved, since lensing does not affect photon numbers), with a mode shifted towards the demagnified regime and a long tail to high magnification. This implies that most sources will be demagnified, inducing an apparently enhanced accelerated expansion, while a few will be highly magnified. The effect is obviously stronger for higher redshift sources since the lower the redshift the less the optical depth of lensing. Note that although the detailed shape of $P(\mu_a)$ is a function of the underlying cosmology, density profile and evolutionary phase of the intervening cosmic structures, the main features discussed previously remain unaltered (e.g. Wang, Holz & Munshi 2002).

We will therefore model the lensing effect using a lognormal magnification distribution, according to appendix A of HL05. The fact that the mean flux, over all different paths of a source, converges to the unlensed value implies that if we had a large number of standard candles densely populating all the redshift bins, the lensing effects would be smoothed out and it would be unnecessary to correct. However, this is not usually the case and therefore we need to take lensing into account (especially for the high-z sources).

Two main effects of lensing will be accounted for the following.

(i) The increase of the distance modulus uncertainty by a further term due to lensing, $\sigma_{\rm eff}$, which was found by HL05 to be a linear function of redshift with $\sigma_{\rm eff} = 0.093z$. For a large number, N, of paths (or equivalently of sources) the lensing distribution is approximately Gaussian with variance σ_N^2 and although the lensing distribution of a single path (source) is non-Gaussian, we can define the effective variance of a single path (or source) as $\sigma^2_{\rm eff} = N\sigma_N^2$. As suggested by HL05 a reasonable $\sigma^2_{\rm eff}/N$ contribution to the total distance modulus variance is given by requiring $N \gtrsim 10$ within z bins of $\sim 0.1z$ width. Note that this is the only lensing-dependent effect that has been taken into account in some of the SNIa-based analyses (e.g. Kowalski et al. 2008; Amanullah et al. 2010).

(ii) The shift of the mode of the distance modulus distribution to demagnified values (fainter) due to lensing. This is an effect that has not yet been taken into account in the SNIa-based studies.

In order to investigate this later effect, and as we have already pointed out previously, we will use the lognormal approximation to the magnification distribution due to its nice analytical properties and its resemblance to the actual magnification distribution (see HL05). If μ_a is the source magnification, then its probability distribution is approximated by

$$P(\mu_a) = \frac{1}{2\pi}\frac{1}{S\mu_a}\exp\left[-\frac{(\ln\mu_a - \langle\ln\mu_a\rangle)^2}{2S^2}\right], \quad (9)$$

with S^2 the variance of $\ln\mu_a$. The mean magnification is given by $\langle\mu_a\rangle = \exp(\langle\ln\mu_a\rangle + S^2/2) = 1$, implying that $\langle\ln\mu_a\rangle = -S^2/2$. Therefore, the probability function is skewed ($\langle\ln\mu_a\rangle < 0$) and determined by only the S parameter. From equation (9) HL05 derived the corresponding flux distribution, which is also lognormal, and then the corresponding magnitude distribution, which is given by

$$P(m) = \frac{1}{\sigma_{\rm m}\sqrt{2\pi}}\exp\left[\frac{(-m - m_0 + b\langle\ln\mu_a\rangle)^2}{2\sigma^2_{\rm m}}\right], \quad (10)$$

with $b = 2.5/\ln 10$ and $\sigma^2_{\rm m} = \sigma^2_{\rm obs} + (bS)^2$. Therefore, we recapitulate that the effects of lensing are

(a) an offset of the mean, given by

$$\langle m\rangle = m_0 + \delta m, \quad (11)$$

where m_0 is the intrinsic (demagnified) magnitude, and $\delta m = -b\langle\ln\mu_a\rangle = bS^2/2$, and

(b) an increase of the variance for which we have that $\sigma^2_{\rm eff} = (bS)^2$ and thus $S^2 = \sigma^2_{\rm eff}/b^2$.

Recalling that for large enough sources (N), in relatively small z bins ($\sim 0.1z$), we have that $\sigma^2_{\rm eff} = N\sigma^2_N$, we obtain that the magnitude offset of sources within the redshift bin is given by

$$\delta m(z) = \frac{\sigma^2_{\rm eff}}{2bN} = \frac{(0.093z)^2}{2bN}, \quad (12)$$

and the total source variance

$$\sigma^2_{\rm m}(z) = \sigma^2_{\rm obs} + (0.093z)^2/N. \quad (13)$$

In Fig. 2 we plot as an example the magnification, flux and magnitude probability distributions for the case of a single source placed at two different redshifts ($z = 1$ and 3) and for an intrinsic observational magnitude uncertainty of $\sigma_{\rm obs} = 0.1$. The intrinsic flux of the source is assumed to be 10^{-17} erg s^{-1} cm^{-2} and the intrinsic apparent magnitude $m = 18$. The main effects discussed previously are clearly seen, i.e. a mode offset towards the demagnification (fainter) regime and an enhanced variance, both increasing with redshift. In Fig. 3 we plot the expected increase of both the mode offset and variance (in magnitudes) as a function of redshift for a single source (left-hand panel). In the right-hand panel of the same figure we plot the suppression of both quantities as we increase the source sampling (the case shown corresponds to a source located at a redshift $z = 3$).

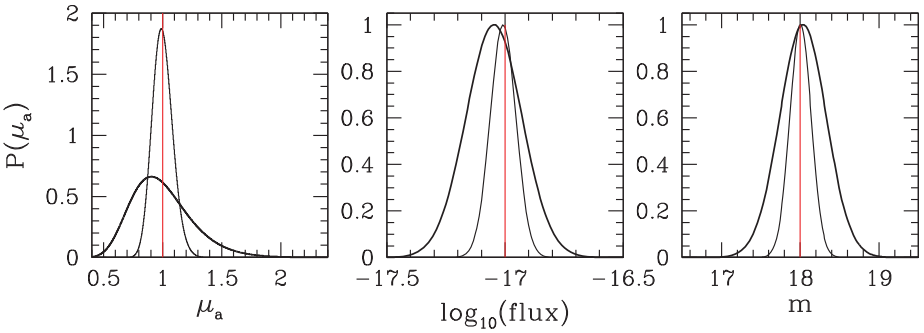

Figure 2. Probability density function of the lensing magnification (left), flux (middle) and magnitude (right) distributions for a source with intrinsic magnitude uncertainty of $\sigma_{\rm int} = 0.1$ at two different redshifts (thin line corresponds to $z = 1$, while the thick line to $z = 3$).

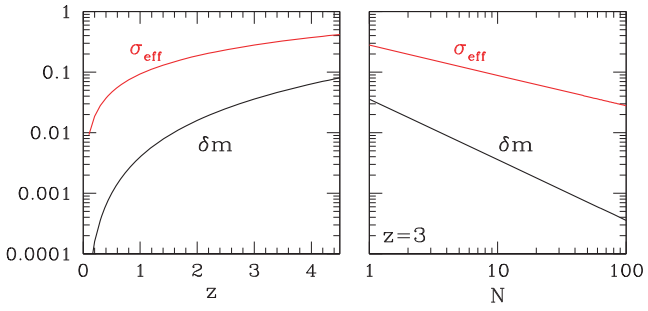

Figure 3. The mode offset (δm) and effective variance ($\sigma_{\rm eff}$) (a) of a source as a function of redshift (left-hand panel) and (b) as a function of the number of sources, N, tracing the same redshift (for this example $z = 3$).

We will therefore correct statistically the distance moduli of observed standard candles (SNIa, GRBs, H II galaxies, etc.) by subtracting an offset $\delta m(z)$ from their raw distance modulus (according to equation 12), within redshift bins of $\sim 0.1z$ width and using as the total distance modulus uncertainty that given by equation (13).

2.3 Best strategy to determine the DE equation of state

2.3.1 Fitting models to the data

We can now proceed with our investigation to find an efficient strategy to put more stringent constraints on the DE equation of state. To this end we have decided to re-analyse two recently compiled SNIa samples, the D07 compilation of 192 SNIa (based on data from Astier et al. 2006; Riess 2007; Wood-Vasey et al. 2007) and the *Constitution* compilation of 397 SNIa (Hicken et al. 2009). Note that the two samples are not independent since most of the D07 is included in the *Constitution* sample.

First, we present in the left-hand panel of Fig. 4 the *Constitution* SNIa distance moduli overplotted (red continuous line) with the theoretical expectation of a flat cosmology with $(\Omega_{\rm m}, w) = (0.27, -1)$. In the inset we plot the distance moduli difference between the SNIa data and the previously mentioned model. To appreciate the level of accuracy needed in order to put constraints on the equation of state parameter, we also plot the distance moduli difference between the reference $(\Omega_{\rm m}, w) = (0.27, -1)$ and the $(\Omega_{\rm m}, w) = (0.27, -0.85)$ models (continuous red and dashed blue line, respectively).

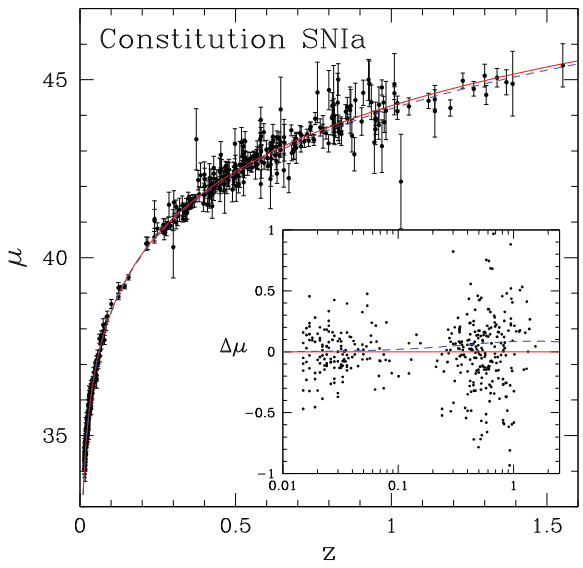

Figure 4. SNIa distance moduli as a function of redshift. Inset panel: distance moduli difference between the best-fitting model (see Table 1) and the SNIa data. The blue dashed line is the corresponding difference between the reference (red continuous line) $(\Omega_{\rm m}, w) = (0.3, -1.04)$ and the $(\Omega_{\rm m}, w) = (0.3, -0.85)$ DE models.

We proceed to analyse the SNIa data by defining the usual likelihood estimator[2] as

$$\mathcal{L}^{\rm SNIa}(\boldsymbol{p}) \propto \exp\left[-\chi^2_{\rm SNIa}(\boldsymbol{p})/2\right], \tag{14}$$

where $\boldsymbol{p}$ is a vector containing the cosmological parameters that we want to fit for, and

$$\chi^2_{\rm SNIa}(\boldsymbol{p}) = \sum_{i=1}^{N} \left[\frac{\mu^{\rm th}(z_i, \boldsymbol{p}) - \mu^{\rm obs}(z_i)}{\sigma_i}\right]^2, \tag{15}$$

where $\mu^{\rm th}$ is given by equation (5), z_i is the observed redshift and σ_i is the distance modulus uncertainty, which includes the observational uncertainty and the gravitational lensing variance (see equation 13). Since in occasions the observational distance modulus uncertainty has the form $\mu^{+\sigma_p}_{-\sigma_n}$, i.e. it is non-symmetric (due to its logarithmic dependence on the flux), we will use a slightly different weighting scheme in the minimization function that takes into account the asymmetric observational uncertainty. Following Barlow (2004), and assuming that the likelihood function of the observed μ, derived from the theoretical $\mu(\boldsymbol{p})$, is a Gaussian, we can use the following weighting scheme of the χ^2 function:

$$\sigma_i = \sigma_1 + \sigma_2[\mu^{\rm th}(\boldsymbol{p}) - \mu^{\rm obs}], \tag{16}$$

with $\sigma_1 = 2\sigma_p\sigma_n/(\sigma_p + \sigma_n)$ and $\sigma_2 = (\sigma_p - \sigma_n)/(\sigma_p + \sigma_n)$. Obviously, when $\sigma_p = \sigma_n$ we recover the usual symmetric error weighting.

In what follows we will constrain our analysis within the framework of a flat ($\Omega_{\rm k} = 0$) cosmology and therefore $\boldsymbol{p} \equiv (\Omega_{\rm m}, w_0, w_1)$. Note that we sample the various parameters on a grid as follows: the matter density $\Omega_{\rm m} \in [0.04, 0.64]$, the equation of state parameter $w \in [-2.0, -0.5]$, while when using a time-dependent equation of state $w_0 \in [0, -2]$ and $w_1 \in [-3, 3]$. The typical step size that we use is 0.0015. Note that the uncertainty of each fitted parameter will be estimated after marginalizing one parameter over the other, providing as its uncertainty the range for which $\Delta\chi^2 \leq 2.3$ (2σ). Such a definition, however, may hide the extent of a possible degeneracy between the two fitted parameters and therefore it is important to visualize the 2D solution space, as indicated in the relevant contour plots.

2.3.2 Larger numbers?

The first issue that we wish to address is how better have we done in imposing cosmological constraints by increasing the available SNIa sample from 181 to 366 (excluding the $z < 0.02$ SNIa),[3] i.e. more than doubling the sample. Table 1 presents various solutions using each of the two previously mentioned samples. Note that since only the relative distances of the SNeIa are accurate and not their absolute local calibration, we always marginalize with respect to the internally derived Hubble constant (for methods that do not need to a priori marginalize over the internally estimated Hubble constant; see e.g. Wei 2008).

[2] Likelihoods are normalized to their maximum values.

[3] We use only SNIa with $z \geq 0.02$ in order to avoid redshift uncertainties due to the local bulk flow (e.g. Hudson et al. 1999 and references therein).

Table 1. Cosmological parameter fits using the SNIa data for a flat prior cosmology. Note that for the case where $\boldsymbol{p} = (\Omega_{\rm m}, w)$, the indicated uncertainties are estimated by fixing one parameter at its best value and allowing the other to vary, providing as its uncertainty the range for which $\Delta\chi^2 \leq 2.3$.

D07			*Constitution*		
w	$\Omega_{\rm m}$	$\chi^2_{\rm min}$/dof	w	$\Omega_{\rm m}$	$\chi^2_{\rm min}$/dof
Raw					
-1	0.287 ± 0.020	186.721/180	-1	$0.285^{+0.015}_{-0.014}$	439.745/365
-1.005 ± 0.076	0.289 ± 0.030	186.721/179	-1.038 ± 0.053	0.300 ± 0.022	439.703/364
Lensing corrected					
-1	0.288 ± 0.020	184.775/180	-1	0.284 ± 0.014	438.263/365
-0.995 ± 0.075	0.286 ± 0.030	184.775/179	-1.036 ± 0.053	0.299 ± 0.022	438.229/364

Regarding the fitted parameters uncertainty, we remind the reader that the definition we use (see above) cannot clearly reveal the extent of the degeneracy between the two parameters. A possible measure of such a degeneracy, beyond inspecting the relevant contour plots, is to also present the whole range of the 1σ contours for each parameter. For example, the corresponding ranges are $\Omega_{\rm m} \in [0.11, 0.42]$ and $\Omega_{\rm m} \in [0.18, 0.40]$ for the D07 and *Constitution* SNIa data sets, respectively, while the corresponding w ranges are $w \in [-0.66, -1.48]$ and $w \in [-0.78, -1.38]$.

Although the derived cosmological parameters are consistent between the two data sets, possibly indicating the robustness of the method, the corresponding goodness of fit (the reduced χ^2) is significantly larger in the case of the *Constitution* set (1.21 compared to 1.045 of the D07 set). This appears to be the outcome of the different approaches chosen in order to join the different contributing SNIa subsets. According to Hicken (private communication) in the case of the D07 the nearby SNeIa were constrained to provide a χ^2/dof $\simeq 1$ by hand, while no such fine-tuning was imposed on the *UNION* set (on which the *Constitution* set is based). A secondary reason could be that the latter set includes distant SNIa which have typically larger distance modulus uncertainties, with respect to those used in D07. Overall, the higher χ^2/dof value of the *Constitution* set should be attributed to a typically lower uncertainty in μ. As a crude test, we have increased by 20 per cent the distance modulus uncertainty of the *Constitution* nearby SNIa ($z \lesssim 0.4$) and indeed we obtain χ^2/dof $\simeq 1.07$, similar to that of D07. To also test whether lensing could have a significant effect on the derived cosmological values, we apply our lensing magnification correction procedure (see Section 2.2) to both SNIa compilations and find a very small and insignificant change of the uncorrected for lensing results (see Table 1, last two rows), but interestingly a slightly better reduced χ^2 value.

In Fig. 5 we can also see that although the SNIa sample has doubled in size, the well-known *banana* shape region of the $(\Omega_{\rm m}, w)$ solution space, indicating the degeneracy between the two cosmological parameters, is roughly the same for both data sets. However, there is a reduction of the size of the solution space when using the *Constitution* SNIa compilation (see also Table 1) at roughly the level expected from Poisson statistics.

A first conclusion is therefore that the increase by $\sim$100 per cent of the *Constitution* sample has not broken the degeneracy in the $(\Omega_{\rm m}, w)$ plane and thus has not provided significantly more stringent constraints to the cosmological parameters. We have further verified that the larger number of SNIa's in the *Constitution* sample are not preferentially located at low redshifts (see inset panel of Fig. 5) – in which case we would not have expected more stringent

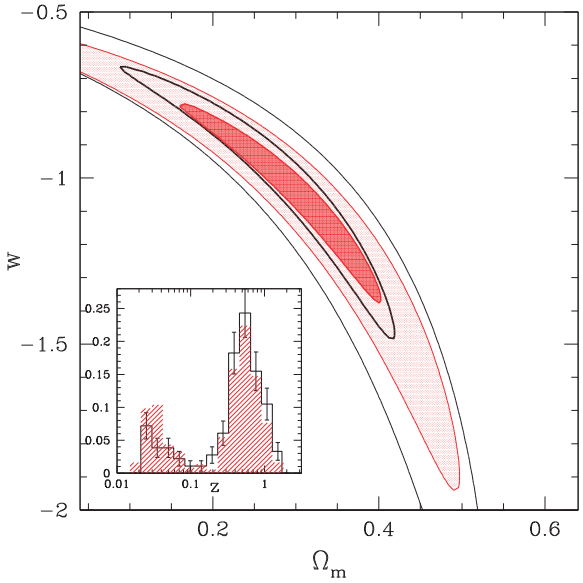

Figure 5. Cosmological parameter solution space using either of the two SNIa data sets (*Constitution*: red shaded contours and D07: black contours). Contours corresponding to the 1 and 3σ confidence levels are shown (i.e. plotted where $-2\ln\mathcal{L}/\mathcal{L}_{\rm max}$ is equal to 2.30 and 11.83, respectively). Inset panel: normalized redshift distributions of the two SNIa data sets (the shaded histogram corresponds to the *Constitution* set).

cosmological constraints using the latter SNIa sample, but they have very similar z distributions.

We already have a strong hint, from the previously presented comparison between the D07 and *Constitution* results, that increasing the number of Hubble relation tracers, covering the same redshift range and with the current level of uncertainties, as in the available SNIa samples, does not appear to be an efficient avenue for providing stringent constraints of the cosmological parameters.

2.3.3 Lower uncertainties or higher z's

We now resort to a Monte Carlo procedure to investigate which of the following two directions, that bracket many different possibilities, provide the required more stringent cosmological constraints:

(i) reduce significantly the distance modulus uncertainties of SNIa, tracing however the same redshift range as the currently available samples, or

(ii) use tracers of the Hubble relation located at redshifts where the models show their largest relative differences ($z \gtrsim 2$), with

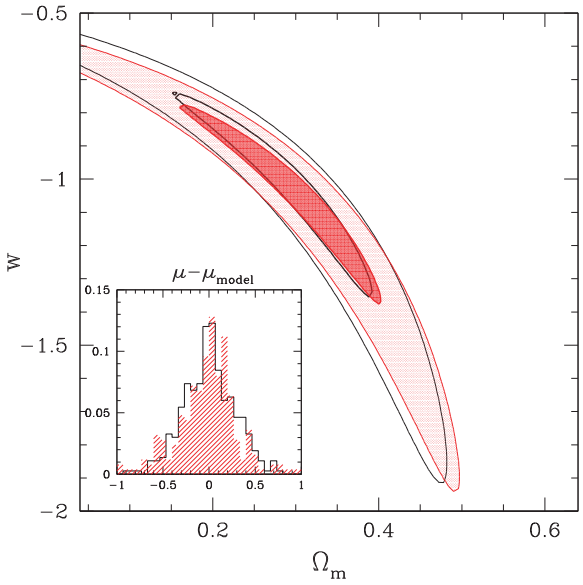

Figure 6. Comparison between the *Constitution* SNIa constraints (red shaded contours) and those derived by a Monte Carlo procedure designed to closely reproduce them (for clarity we show only contours corresponding to 1 and 3σ confidence levels). Inset panel: the *Constitution* SNIa distance modulus deviations from the best-fitting model ($\Omega_{\rm m}$, w) $\simeq$ (0.30, −1.01); see Table 1 – and a random realization of the model deviations (red shaded histogram).

distance modulus uncertainties comparable to that of the highest redshift SNeIa ($\langle\sigma_\mu\rangle \simeq 0.4$). At such large redshifts, however, we expect that the gravitational lensing magnification/demagnification effects will be significant and therefore we will also use the algorithm presented in Section 2.2 to statistically degrade the intrinsic source flux and investigate its effects on the derived cosmological parameters.

The Monte Carlo procedure is based on using the observed high-z SNIa distance modulus uncertainty distribution (σ_μ) and a model to assign random μ deviations from a reference $H(z)$ function, that reproduces exactly the original banana-shaped contours of the ($\Omega_{\rm m}$, w) solution space of Fig. 5, or in the case of the CPL model of the DE equation of state the corresponding contours in the w_0, w_1 solution space. Indeed, after a trial and error procedure we have found that by assigning to each SNIa (using their true redshift) a distance modulus deviation ($\delta\mu$) from a reference model having a Gaussian distribution with zero mean and variance given by the observed $\langle\sigma_\mu\rangle^2$, and using as the relevant individual distance modulus uncertainty the following $\sigma_i^2 = \sqrt{(1.2\delta\mu_i)^2 + \phi^2}$ (with ϕ a random Poisson deviate within [−0.01, 0.01]) we reproduce exactly the banana-shaped solution range of the reference model. This can be seen clearly in Fig. 6, where we plot the original *Constitution* SNIa solution space (red shaded contours) and the model solution space (black contours). In the inset panel we show the distribution of the true SNIa deviations from the best-fitted model as well as a random realization of the corresponding model deviations.

Armed with the above procedure we can now address the questions posed previously. First, we reduce to half the random deviations of the SNIa distance moduli from the reference model (with the corresponding reduction of the relevant uncertainty, σ_i). The results of the likelihood analysis can be seen in the left-hand panel of Fig. 7. There is a reduction of the range of the solution space, but indeed quite a small one. Secondly, we add to the *Constitution* SNIa sample, a mock subsample of 76 high-z tracers with a distance modulus mean uncertainty of $\langle\sigma_\mu\rangle \simeq 0.5$ (corresponding to that of the current H II galaxy data) randomly distributed between $2 \lesssim z \lesssim 3.5$, i.e. in a range where the largest deviations between the different cosmological models occur (see Fig. 1). We now find a significantly reduced solution space (central panel of Fig. 7), which shows that indeed by increasing the $H(z)$ tracers by a few tens, at those redshifts where the largest deviations between models occur, can have a significant impact on the recovered cosmological parameter solution space. If we include the expected lensing degradation of the distance modulus (according to equation 12), then we observe (right-hand panel of Fig. 7) a slightly worsening of the solution space, but still significantly smaller than that of the left-hand panel of Fig. 7.

The main conclusion of the previous analysis is that a more efficient strategy to decrease the uncertainties of the cosmological parameters, based on the Hubble relation, is to use standard candles which trace also the redshift range $2 \lesssim z \lesssim 3.5$. However, in such a case the effects of gravitational lensing can be severe, especially for small number of high-z tracers, and therefore it is necessary to be taken into account.

2.3.4 *Figure of merit analysis*

In order to study the relation between the number of high-z tracers used and the corresponding reduction of the cosmological parameter solution space, we will use the figure of merit (FoM; Bassett 2005; Albrecht et al. 2006; Bueno Sanchez, Nesseris & Perivolaropoulos 2009), defined as the reciprocal area of the 2σ contour (i.e. where $-2\ln\mathcal{L}/\mathcal{L}_{\rm max} = 6.14$) in the parameter space of any two degenerate cosmological parameters [e.g. ($\Omega_{\rm m}$, w) for the QDE model or (w_0, w_1) for the CPL model], and which has been found to be a useful measure of the effectiveness of a data set in constraining cosmological parameters. A larger FoM indicates a greater accuracy in constraining the cosmological parameters.

Here we will use a slightly different quantity, which we call 'reduction factor' and is indicated by S, defined as the ratio of the FoM of the SNIa+high-z Hubble relation solution to that of only the SNIa (in both cases we use the *Constitution* set), in order to study the question of how better can we constrain the cosmological parameter space, when adding $N_{\text{high-}z}$ high-z tracers of the Hubble relation, with respect to the best current SNIa data set as a function of the number of high-z tracers. For example a value $S = 2$ indicates that the FoM based on the SNIa+high-z Hubble relation is half of that based on the *Constitution* SNIa data set, i.e. the 2σ range of the solution space is reduced by a factor of 2.

In Fig. 8 we present the results of our analysis as a function of the number of high-z tracers for the QDE model. We present results only for the realistic lensing degradation case and for two different values of the distance modulus mean observational uncertainty, ranging between a pessimistic ($\langle\sigma_\mu\rangle = 0.5$; open circles) and an optimistic ($\langle\sigma_\mu\rangle = 0.25$; filled points) value.

It is evident that including even a small number of high-z tracers we can reduce significantly the cosmological parameter solution space. There is a roughly linear relation between S and the number of high-z tracers used, $N_{\text{high-}z}$, which depends obviously on the distance modulus mean uncertainty, $\langle\sigma_\mu\rangle$ and on whether one uses in addition to the high-z tracers also the lower redshift SNIa data.

It is also interesting to note that the high-z H II galaxies could constrain cosmological parameters with the level of accuracy provided by current SNIa data sets (for $N_{\text{high-}z} \gtrsim 200$) and thus lift any doubts that arise from the fact that SNeIa are the only reliable tracers of the Hubble relation used to-date. Of course the above

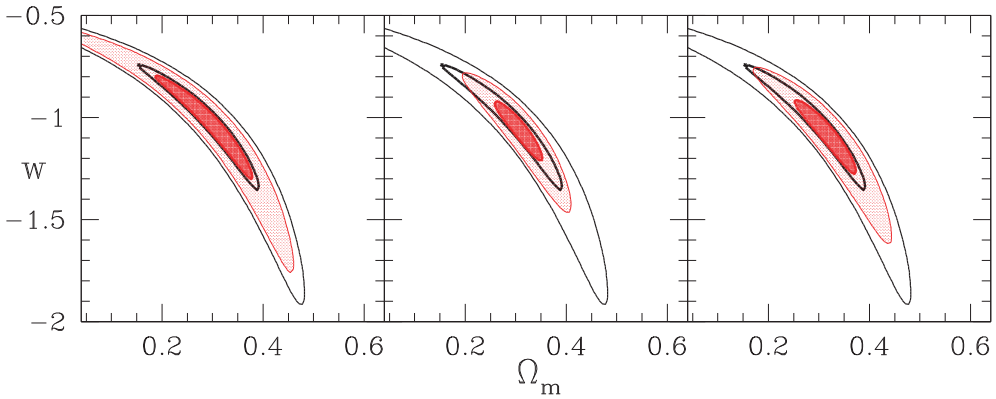

Figure 7. Comparison of the model *Constitution* SNIa constraints (black contours) with those (filled contours) derived by reducing to half their uncertainties (left-hand panel), with those derived by adding a sample of 76 high-z tracers ($2 \lesssim z \lesssim 3.5$) with a distance modulus mean uncertainty of $\langle\sigma_\mu\rangle \simeq 0.5$ and no lensing degradation (central panel), and with those by including statistically the expected lensing degradation (right-hand panel). For clarity we show only contours corresponding to the 1 and 3σ confidence levels.

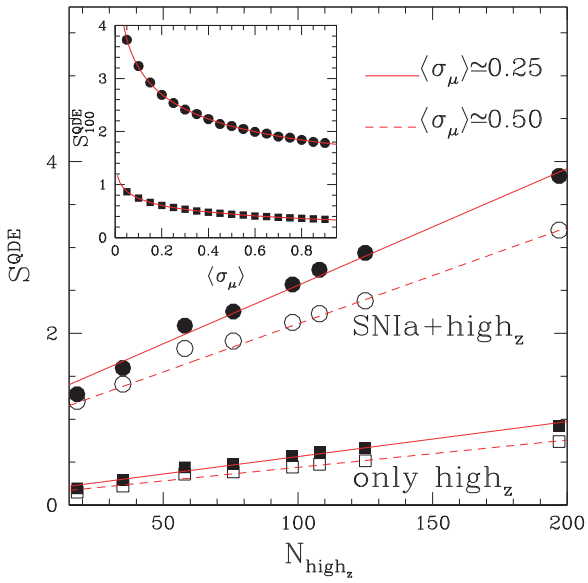

Figure 8. The 'reduction' parameter S, indicating the factor by which we reduce the 2σ contour area of the cosmological parameters (Ω_m, w) solution space (QDE model) as a function of the number of high-z tracers ($2 < z < 3.5$) of the Hubble relation and for two different values of the mean intrinsic distance modulus scatter (as indicated in the plot). Circular points correspond to using the high-z tracers together with the current best SNIa data set, while the squares to using only the high-z tracers (and a local $z < 0.2$ *calibration* sample). Inset panel: the 'reduction' parameter for the case of using 100 high-z tracers as a function of the mean distance modulus uncertainty, $\langle\sigma_\mu\rangle$. The lines correspond to logarithmic fits to the data (see text).

relatively large number of high-z H II galaxies can be significantly reduced by including an intermediate population of H II galaxies, i.e. tracing similar depths as the current SNIa samples ($z \lesssim 1$). In such a case the expected values of S will be intermediate between the *only high-z* and *SNIa–high-z* curves of Fig. 8. For example, a realistic case of a sample with 80 $0.2 < z < 1$ and 60 $z \gtrsim 2$ H II galaxies and a rms distance modulus uncertainty of $\sim$0.35 will provide similar constraints as the current SNIa based analyses ($S \simeq 1$).

In order to quantify the previous results and provide a tool to estimate the number of high-z tracers necessary to reduce the current SNIa solution space by a given factor, taking into account the whole parameter space, we first normalize the S values by that given for, say, $N_{\text{high-}z} = 100$ (S_{100}). We then quantify how S_{100} depends on $\langle\sigma_\mu\rangle$, which is shown in the inset panel of Fig. 8. The continuous curves are logarithmic fits to the data, which are given by the following equations:

$$S_{100}^{\rm QDE} \simeq \begin{cases} 1.87\log_{10}(\langle\sigma_\mu\rangle^{-1} + 0.74) + 1.28 & \text{SNIa + high-}z, \\ 0.44\log_{10}(\langle\sigma_\mu\rangle^{-1} + 0.15) + 0.30 & \text{only high-}z. \end{cases} \quad (17)$$

Then, in order to obtain the number of high-z tracers, $N_{\text{high-}z}$, necessary to reduce the cosmological solution space (in the QDE model) by a factor S, we fit the normalized value S/S_{100} and find

$$N_{\text{high-}z} \simeq \begin{cases} 187\ S/S_{100} - 88 & \text{SNIa + high-}z, \\ 139\ S/S_{100} - 39 & \text{only high-}z, \end{cases} \quad (18)$$

which has a typical uncertainty of $\sigma_N \simeq \pm 5$ for both the SNIa+high-z and only high-z cases. The continuous (red) lines in the left-hand panel of Fig. 8 are derived from equations (17) and (18) for $\langle\sigma_\mu\rangle = 0.25$ and 0.5, and it is evident that they reproduce extremely well the observed S values (points). As an example, we can ask how many high-z tracers, with say $\langle\sigma_\mu\rangle = 0.4$, do we need to add to the current SNIa data set in order to reduce by a factor of 2 ($S = 2$) the current SNIa QDE solution space. Using equations (17) and (18) we find $N_{\text{high-}z} \simeq 80$, which drops to $\sim$60 for $\langle\sigma_\mu\rangle = 0.25$. It is therefore interesting to point out that a reduction by a factor of 2 in the distance modulus uncertainty of the high-z tracers (which is really a non-trivial aim) can be compensated by a relatively small increase in the number of high-z tracers.

Repeating the previous analysis for the case of an evolving DE equation of state (CPL; as in equation 2), and after marginalizing with respect to Ω_m, we also find a reduction of the (w_0, w_1) solution space, when we include the high-z tracer subsample (Fig. 9), but significantly smaller than that of the QDE parametrization. We can again estimate what is the necessary number of high-z tracers, $N_{\text{high-}z}$, having a mean distance modulus error of $\langle\sigma_\mu\rangle$, in order to reduce the cosmological (w_0, w_1) solution space by a factor S. Again using a parametrization based on the value of S for $N_{\text{high-}z} = 100$, we have that

$$S_{100}^{\rm CPL} \simeq \begin{cases} 0.49\log_{10}(\langle\sigma_\mu\rangle^{-1} + 0.65) + 1.09 & \text{SNIa + high-z}, \\ 0.20\log_{10}(\langle\sigma_\mu\rangle^{-1} + 0.69) + 0.22 & \text{only high-}z \end{cases} \quad (19)$$

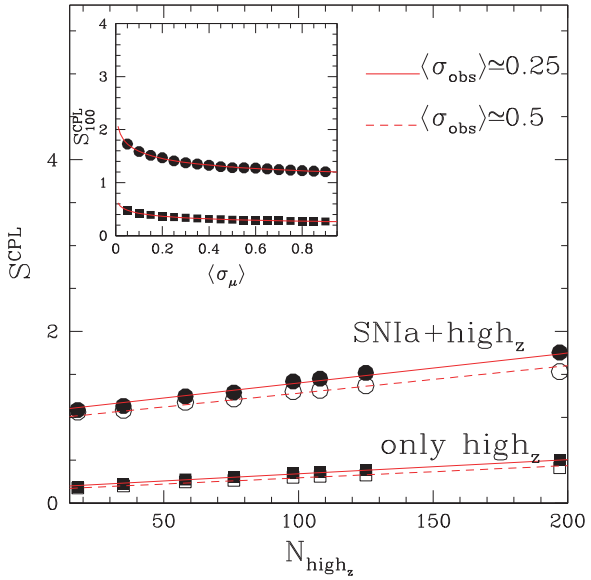

Figure 9. As in Fig. 8 but for an evolving DE equation of state (CPL model) and after marginalizing with respect to Ω_m. The input cosmological model has $(\Omega_m, w_0, w_1) = (0.3, -0.98, -0.48)$. The axes scale has been kept as in Fig. 8 in order to appreciate the significant reduction of efficiency of the high-z Hubble relation in providing cosmological constraints for the CPL model.

and

$$N_{\text{high-}z} \simeq \begin{cases} 404\ S/S_{100} - 300 & \text{SNIa + high-z,} \\ 211\ S/S_{100} - 106 & \text{only high-}z, \end{cases} \quad (20)$$

with a typical uncertainty of $\sigma_N \simeq \pm 17$ and ± 7 for the SNIa+high-z and only high-z cases, respectively. These results imply than in order to reduce by a factor of 2 ($S = 2$) the current SNIa CPL solution space using high-z tracers with $\langle\sigma_\mu\rangle = 0.35$, one needs $N_{\text{high-}z} \simeq 300$ and 1200 for the SNIa+high-z and only high-z tracers case, respectively. The latter value can be significantly reduced if we include an intermediate-redshift ($0.2 \lesssim z \lesssim 1$) H II sample, as discussed also for the QDE case previously. For example, using a sample of 80 such intermediate-z H II galaxies reduces this number by a factor of 2. In any case, the large number of high-z tracers of the Hubble expansion, needed to effectively constrain the CPL equation of state, renders this task rather unrealistic. Therefore, in order to provide stringent cosmological constraints for the CPL model (i.e. the values of w_0 and w_1), it would be necessary (a) to combine the high-z Hubble relation with that of current SNIa data, and (b) to join the Hubble relation analysis with other cosmological tests, like the one that is an integral part of our proposal, i.e. the clustering of X-ray AGN. Of course other cosmological probes, like BAOs, can and should be used as well.

We now draw the main conclusions of our Monte Carlo analysis are as follows.

(i) Even a small number of high-z ($2 \lesssim z \lesssim 3.5$) tracers of the Hubble expansion can reduce significantly the QDE model parameter solution space.

(ii) For the case of the CPL model, in order to reduce the (w_0, w_1) solution space, provided by the current *Constitution* SNIa set, by the same amount as in the corresponding QDM model, one needs three or more as many high-z Hubble expansion tracers.

(iii) It appears that the effort to reduce significantly the current level of random distance modulus scatter of H II galaxies is not as important as it is to increase the number of high-z H II galaxies, unless one is able to reduce it to $\langle\sigma_\mu\rangle \lesssim 0.1$–$0.2$ (as can be seen in the inset panel of Fig. 8).

2.4 A high-z Hubble relation tracer: H II galaxies

H II galaxies, compact extragalactic objects experiencing massive bursts of star formation, have a high-luminosity per unit mass, in large part concentrated in a few strong emission lines in the optical rest frame. This ensures that the first, obvious, requirement for a standard candle to be usable at very large distances is met.

The potential use of H II galaxies as distance indicators stems from the fact that as one increases the mass of the young stellar component, not only the ionizing output increases, but also the turbulent velocity of the gas, which is indicative of supersonic motions in the gas in the stellar gravitational potential, becomes larger. This effect induces a correlation between the integrated luminosity in a nebular hydrogen recombination line, e.g. $L(\mathrm{H}\beta)$, which is proportional to the number of ionizing photons, and the linewidth σ.

Terlevich & Melnick (1981) found the first observational confirmation of a correlation between Hβ luminosity and line profile width for giant extragalactic H II regions and H II galaxies, with residuals that are correlated with the nebular metallicity. Subsequent work by Melnick et al. (1987, 1988) was devoted to obtain a calibration of this correlation in order to make it suitable for distance measurements.

The distance indicator, defined as $M_z = \sigma^5/(\mathrm{O/H})$ with O/H the oxygen abundance of the nebular gas, provides the predicted luminosity from the relation

$$\log L(\mathrm{H}\beta) = \log M_z + P_0, \quad (21)$$

where the zero-point $P_0 = 29.60$ was originally defined from a sample of 14 giant extragalactic H II regions (Melnick et al. 1988) and from which they obtained $H_0 = 80 \pm 5\,\mathrm{km\,s^{-1}\,Mpc^{-1}}$. Obviously, a critical prerequisite for using such scaling relations as distance estimators is an accurate calibration of their zero-points. Note that a semi-empirical upper limit of $\sigma = 65\,\mathrm{km\,s^{-1}}$ has been proposed for suitable galaxies, which can be explained by the requirement that H II galaxies are powered by clusters of coeval starbursts with their dynamics dominated by pressure and not rotation.

The $L(\mathrm{H}\beta)$–σ relation has been shown to hold also at large redshifts (Koo et al. 1996; Pettini et al. 2001; Erb et al. 2003). Melnick et al. (2000) showed that H II-like starburst galaxies up to $z \simeq 3$, satisfy the $L(\mathrm{H}\beta)$–σ relation, opening the possibility of using the relation to measure cosmological parameters. They derived the following distance modulus relation for H II galaxies:

$$\mu = 2.5\log(\sigma^5/F_{\mathrm{H}\beta}) - 2.5\log(\mathrm{O/H}) - A_{\mathrm{H}\beta} + Z_0, \quad (22)$$

where $F_{\mathrm{H}\beta}$ and $A_{\mathrm{H}\beta}$ are the flux and extinction in Hβ, respectively. The originally determined zero-point was $Z_0 = -26.18$ and the rms distance modulus dispersion was found to be $\sim$0.52 mag. Although, such an rms uncertainty is larger than what is obtained with SNIa, the advantage of using H II galaxies is that we can reach a much larger redshift limit ($z \sim 4$ versus $z \sim 1.7$).

Using recent galaxy distance determinations we should be able to better determine the zero-point of the distance indicator, Z_0. To this end we have repeated the original analysis of Melnick et al. (1988, 2000), using Cepheid and RR Lyrae distance determinations and indeed the rms scatter of the distance indicator relation is reduced by $\sim$7 per cent while $P_0 = 29.44$. This results in a reduction by $\sim$0.42 mag of the zero-point (i.e. $Z_0 = -26.60$), which provides

results consistent with $H_0 = 73\,\mathrm{km\,s^{-1}\,Mpc^{-1}}$ (Chávez et al., in preparation).

It should also be mentioned that there are some systematic effects than can bias distances obtained with the $L(\mathrm{H}\beta)$–σ relation, in particular differences in the ages of the stellar populations, contamination from underlying old stellar components, or different extinction laws. To some extent these effects can be mitigated by using the equivalent widths of the lines to select only very young objects, and the use of modern instrumentation that allows a precise control of the size, orientation and location of the spectrograph slits. Still the observations remain challenging and require a high level of planning and control.

We are at the process of completing an investigation of these effects by using high-resolution spectroscopy of a relatively large number of Sloan Digital Sky Survey (SDSS) low-z H II galaxies with a wide range of relevant parameters (Hβ equivalent widths and luminosities, metal content and local overdensity) in an attempt to understand systematics and to reduce the scatter of the distance estimator (Chávez et al., in preparation).

Most high-z H II galaxies known until recently were found in broad-band searches aimed mostly to search for Lyman break galaxies, which means that they generally have relatively strong continua. Still, a substantial fraction present strong emission lines making them ideal for our distance estimator (see e.g. Erb et al. 2006a,b) Furthermore, deep slit-less surveys using the Wide Field Camera 3 (WFC3) on *Hubble Space Telescope* (*HST*) and narrow-band filters at Subaru have revealed substantial numbers of H II galaxies with large equivalent widths (i.e. strong emission lines and weak continua) at intermediate and high redshifts (Yamada et al. 2005; Kazaku, Cowie & Hu 2007; Atek et al. 2010; Nestor et al. 2011; Straughn et al. 2011; Xia et al. 2011). In all, the present sample has more than 400 H II galaxies covering the redshift range $0.5 < z < 3.7$ with about 100 in the range $3.0 < z < 3.7$ and about 150 at $z \sim 2$.

Summarizing, the use of H II galaxies to trace the Hubble relation, as an alternative to the traditionally used SNIa, is based on the following facts.

(a) Local and high-z H II galaxies define a phenomenological relation between Hβ luminosity, velocity dispersion and metallicity as traced by O/H that holds out to cosmological distances. Thus, H II galaxies can be used as alternative tracers of the Hubble expansion.

(b) H II galaxies can be readily observed at much larger redshifts than those currently probed by SNIa samples.

(c) It is at such higher redshifts that the differences between the predictions of the different cosmological models appear more vividly (see Fig. 1).

A more recent application using 15 starburst galaxies with redshift in the range $z = 2.17$–3.39 has been carried out by Siegel et al. (2005) in an attempt to constrain cosmological parameters, but the resulting constraints are rather weak. They found $\Omega_\mathrm{m} = 0.21^{+0.30}_{-0.12}$ for a Λ-dominated Universe. Clearly, the errors are still large, and up to this point the results are not competitive with SNIa.

We have performed our own re-analysis of this data set, following a similar procedure to that applied to the SNIa data in the previous sections, but using the newly derived value of Z_0 in equation (22), allowing for the asymmetric uncertainties of the H II-galaxy distance moduli and correcting for the effects of gravitational lensing, according to Section 2.2. Furthermore, we have updated the values of the stellar velocity dispersion and its uncertainty, for some of the galaxies in the Siegel et al. sample, according to Erb et al. (2006a).

Table 2. Cosmological parameter fits using the Siegel et al. H II galaxies and the newly derived zero-point Z_0 (equation 22). The QDE equation of state parameter, w, remains completely unconstrained by the current analysis.

w	Ω_m	χ^2_min/dof
-1	$0.198^{+0.051}_{-0.032}$	53.057/14
Unconstrained	$0.280^{+0.048}_{-0.038}$	53.849/13
Excluding two galaxies with tilted emission lines		
-1	$0.224^{+0.063}_{-0.038}$	43.119/12
Unconstrained	$0.310^{+0.052}_{-0.046}$	42.954/11

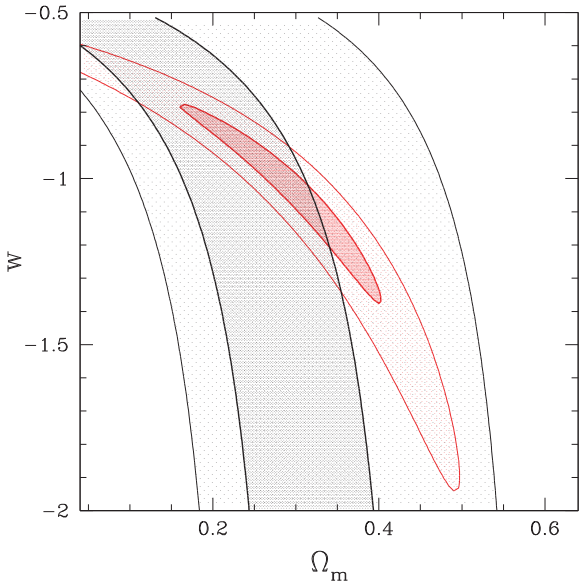

Figure 10. The H II galaxy QDE constraints (in the Ω_m, w plane) based on the Siegel et al. sample after excluding two H II galaxies showing strong indications for a rotational velocity component. Although the constraints are weak, leaving completely unconstrained the value of w, they are consistent at a $\sim 1\sigma$ level with the SNIa results (thin red contours).

The resulting constraints on the (Ω_m, w) plane are indicated in the first two rows of Table 2, while in the last two rows (and in Fig. 10) we present results after excluding two H II galaxies (Q1700−MD103 and SS A22a−MD41) that show indications of a significant rotational velocity component (derived from the tilted emission lines; Erb et al. 2006a), which contaminates the estimate of their velocity dispersion.

Our results show that the derived Ω_m values, independent of the value of w, are towards the lower end of the generally accepted range, while when excluding the two rotating galaxies the fitted Ω_m parameter moves towards higher values, while there is also a decrease of the value of the corresponding reduced χ^2.

In any case, the main qualitative result of our H II-galaxy-based analysis is that although the constraints in the (Ω_m, w) plane are consistent with those of the *Constitution* SNIa analysis, as can be seen in Fig. 10, the provided cosmological parameter uncertainties are significantly larger and the degeneracy between Ω_m and w is even more exacerbated. These results clearly indicate that the

distance indicator for H II galaxies can become highly competitive provided

(i) we increase the number of available high-z ($z \gtrsim 2$) H II galaxies, but it is important to cover also the $0.2 < z < 1$ range (as shown in Section 2.3.4);

(ii) we apply the estimator to a significant sample of bona-fide high-redshift H II galaxies selected by the strength of their emission lines to ensure no contamination by rotation and/or underlying old stellar populations;

(iii) we minimize all possible sources of systematic and random errors.

3 COSMOLOGICAL PARAMETERS FROM THE CLUSTERING OF X-RAY AGN

The method used to put cosmological constraints, based on the clustering of some extragalactic mass tracer (Matsubara 2004; BP09, and references therein), consists in comparing the observed spatial or angular clustering with that predicted by different primordial fluctuations power spectra, in the latter case using also Limber's integral equation (Limber 1953) to invert the spatial to angular clustering. By minimizing the differences of the observed and predicted correlation function, one can constrain the cosmological parameters that enter in the power spectrum determination as well as in Limber's inversion. Using the latter we can relate the angular and spatial clustering of any extragalactic population under the assumption of power-law correlations and the small angle approximation.

We have chosen X-ray-selected AGN as a tracer of the large-scale structure, in order to perform the previously described analysis, for the following reasons.

(a) X-ray-selected AGN can be detected out to high redshifts (the peak of their z distribution is $\sim$1) and thus trace the distant density fluctuations providing a further anchor of the evolution parameter at a redshift other than $z \sim 0$, which most galaxy samples trace to-date.

(b) AGN selected through their X-ray emission (and not in the optical) provide a relatively unbiased census of the AGN phenomenon, since obscured AGN, largely missed in optical surveys, are included in X-ray surveys.

(c) Furthermore, determining the clustering at $\langle z \rangle \sim 1$ and $z \sim 0$, one can put better constraints on the cosmic evolution of the AGN phenomenon and the evolution of the relation between AGN activity and dark matter (DM) halo hosts (e.g. Mo & White 1996; Sheth, Mo & Tormen 2001), and finally also on the cosmological parameters and the DE equation of state (e.g. Basilakos & Plionis 2005, 2006, 2010; BP09).

3.1 Clustering of X-ray AGN: biases and systematics

The earlier *ROSAT*-based analyses (e.g. Boyle & Mo 1993; Vikhlinin & Forman 1995; Carrera et al. 1998; Akylas, Georgantopoulos & Plionis 2000; Mullis et al. 2004) provided conflicting results on the nature and amplitude of high-z AGN clustering. With the advent of the *XMM* and *Chandra* X-ray observatories, many groups have attempted to settle this issue, but in vain. Different surveys have provided again a multitude of conflicting results, intensifying the debate (e.g. Manners et al. 2003; Yang et al. 2003, 2006; Basilakos et al. 2004, 2005; Gilli et al. 2005; Gandhi et al. 2006; Puccetti et al. 2006; Carrera et al. 2007; Miyaji et al. 2007; Coil et al. 2009; Starikova et al. 2010). However, strong indications exist for a flux-limit-dependent clustering, interpreted as an X-ray luminosity dependent clustering, which appears to remove most of the above inconsistencies (Plionis et al. 2008). Such a luminosity-dependent clustering trend was recently reported also by Cappelluti et al. (2010) and Krumpe, Miyaji & Coil (2010).

Furthermore, there are indications for a quite large high-z AGN clustering length, reaching values $\gtrsim 10\,h^{-1}$ Mpc at the brightest flux limits (e.g. Basilakos et al. 2004, 2005; Puccetti et al. 2006; Plionis et al. 2008; Cappelluti et al. 2010), which, if verified, has important consequences for the AGN bias evolution and therefore for the evolution of the AGN phenomenon (e.g. Miyaji et al. 2007; Basilakos, Plionis & Ragone-Figueroa 2008, hereafter BPR08). An independent test of these results would be to establish that the environment of high-z AGN is associated with large DM haloes, which being massive should be more clustered (work in progress).

It is also important to understand and overcome the shortcomings and problems that one is facing in order to reliably and unambiguously determine the clustering properties of the X-ray-selected AGN. Such a list of problems includes the effects of cosmic variance, the so-called amplification bias, the reliability of the $\log N$–$\log S$ distribution of the X-ray AGN luminosity function, etc. (see discussion in Plionis et al. 2009).

Recently, Ebrero et al. (2009b) derived the angular correlation function of the soft (0.5–2 keV) X-ray sources using 1063 *XMM–Newton* observations at high galactic latitudes (2*XMM* survey). A full description of the data reduction, source detection and flux estimation are presented in Mateos et al. (2008). Note that the survey contains $\sim$30 000 soft-band point sources within an effective area of $\sim$125.5 deg^2 (for $f_x \geq 1.4 \times 10^{-15}$ erg cm^{-2} s^{-1}). The large area covered and the corresponding large number of X-ray sources ensure that the previously mentioned cosmic variance effects are minimized. However, further details regarding the various biases that should be taken into account (the amplification bias and integral constraint), the survey luminosity and selection functions as well as issues related to possible non-AGN contamination, which are estimated to be $\lesssim$10 per cent, can be found in Ebrero et al. (2009a).

3.2 Cosmology from the 2*XMM* angular clustering

An optimal approach to unambiguously determine the clustering pattern of X-ray-selected AGN would be to determine both the angular and spatial clustering pattern. The reason being that various systematic effects or uncertainties enter differently in the two types of analyses. On the one side, using the angular two-point correlation function, w(θ), and its Limber inversion, one bypasses the effects of redshift-space distortions and uncertainties related to possible misidentification of the optical counterparts of X-ray sources. On the other side, using spectroscopic or accurate photometric redshifts to measure the spatial, $\xi(r)$, or projected, $w_p(\theta)$, two-point correlation function, one bypasses the inherent necessity, in Limber's inversion of w(θ), of assuming a source redshift-selection function (for the determination of which one uses the integrated X-ray source luminosity function, different models of which exist).

The basic integral equation relating the angular and spatial correlation functions is

$$w(\theta) = 2\frac{H_0}{c}\int_0^\infty \left(\frac{1}{N}\frac{dN}{dz}\right)^2 E(z)\,dz \int_0^\infty \xi(r,z)\,du, \qquad (23)$$

where dN/dz is the source redshift distribution, estimated by integrating the appropriate source luminosity function (in our case that of Ebrero et al. 2009a), folding in also the area curve of the survey. Note that to derive the spatial correlation length from equation (23), it is necessary to model the spatial correlation function as a power

law, assume the small angle approximation as well as a cosmological background model. The latter is provided by the function $E(z)$ (equation 4), which for a flat background and the QDM equation of state, it takes the form

$$E(z) = [\Omega_{\rm m}(1+z)^3 + (1-\Omega_{\rm m})(1+z)^{3(1+w)}]^{1/2}. \quad (24)$$

The AGN spatial correlation function can be written as

$$\xi(r,z) = (1+z)^{-(3+\epsilon)} b^2(z) \xi_{\rm DM}(r), \quad (25)$$

where $b(z)$ is the evolution of the linear bias factor (e.g. Matarrese et al. 1997; Mo & White 1996; Sheth & Tormen 1999; Basilakos & Plionis 2001, 2003; BPR08; Tinker et al. 2010; Ma et al. 2011), ϵ is a parameter related to the model of AGN clustering evolution (e.g. de Zotti et al. 1990) and $\xi_{\rm DM}(r)$ is the corresponding correlation function of the underlying DM distribution, given by the Fourier transform of the spatial power spectrum $P(k)$ of the matter fluctuations, linearly extrapolated to the present epoch:

$$\xi_{\rm DM}(r) = \frac{1}{2\pi^2} \int_0^\infty k^2 P(k) \frac{\sin(kr)}{kr} \, {\rm d}k. \quad (26)$$

The CDM power spectrum is given by $P(k) = P_0 k^n T^2(\Omega_{\rm m}, k)$, with $T(\Omega_{\rm m}, k)$ the CDM transfer function (Bardeen et al. 1986; Sugiyama 1995), $n \simeq 0.967$ and a baryonic density of $\Omega_{\rm b} h^2 = 0.02249$, following the 7-year *Wilkinson Microwave Anisotropy Probe* (*WMAP*) results (Komatsu et al. 2011). The normalization of the power spectrum, P_0, can be parametrized by the rms mass fluctuations on $R_8 = 8\,h^{-1}$ Mpc scales (σ_8), according to

$$P_0 = 2\pi^2 \sigma_8^2 / \Psi(\Omega_{\rm m}, R_8), \quad (27)$$

with

$$\Psi(\Omega_{\rm m}, R_8) = \int_0^\infty k^{n+2} T^2(\Omega_{\rm m}, k) W^2(kR_8) \, {\rm d}k \quad (28)$$

and $W(kR_8) = 3({\rm sin}kR_8 - kR_8 {\rm cos}kR_8)/(kR_8)^3$.

Evidently, the essential parameters needed to characterize any QDE cosmological model are $\Omega_{\rm m}, w, \sigma_8$ and H_0. Regarding the Hubble constant we will use the *WMAP*7 results (Komatsu et al. 2011), which practically coincide with those of the *HST* key project (Freedman et al. 2001), i.e. $h = H_0/100 = 0.704$, while regarding the σ_8 normalization of the CDM power spectrum we will use the extrema of the range provided by the recent analysis of SDSS luminous red galaxies (LRGs) for a range of DE equations of state ($\sigma_{\rm b} \in [0.78, 0.81]$; Sánchez et al. 2009). Note that the upper limit of the above range corresponds to the *WMAP*7 ΛCDM value (Komatsu et al. 2011).

Furthermore, to estimate the predicted QDE model correlation function of the underlying mass, $\xi_{\rm DM}(r, z)$, in order to compare it with the observed AGN clustering, it is necessary to deal with the following three issues.

(i) *Clustering evolution model*. As discussed earlier (see equation 25), in order to estimate the expected clustering of any mass tracer it is important to assume a clustering evolution model (e.g. de Zotti et al. 1990), which is encapsulated in the value of the parameter ϵ. A value $\epsilon = -1.2$ corresponds to a constant in comoving coordinates clustering model, while a value $\epsilon = -3$, to a constant in physical coordinates. According to Kundić (1997) and Basilakos & Plionis (2005, 2006) we will use the former value of ϵ (although we have also tested the effects of using $\epsilon = -3$).

(ii) *Bias evolution model*. We need to calibrate the parameters of the bias evolution model to each cosmological model. Although a large number of bias evolution models have been proposed in the literature (see Papageorgiou, Plionis & Basilakos, in preparation, for a comparison of different models), we use here the approach of Basilakos & Plionis (2001, 2003) which was extended to QDE cosmological models in BPR08. This model is based on linear perturbation theory and the Friedmann–Lemaitre solutions of the cosmological field equations, and includes also the effects of interactions and merging of the mass tracers. Its analytical form has been derived for the QDE cosmological models, and its generalization to the CPL and alternative gravity cosmological models is underway (Basilakos et al., in preparation). Considering that each X-ray AGN is hosted by a DM halo of mass $M_{\rm h}$, we can analytically predict its bias evolution behaviour within the QDE models. Conversely fitting the model to observations, we can determine the mass of the DM halo within which AGN live (for more details see Basilakos & Plionis 2010).

For the case of a spatially flat cosmological model, our bias evolution model has the following form:

$$b(M_{\rm h}, z) = \mathcal{C}_1(M_{\rm h}) E(z) + \mathcal{C}_2(M_{\rm h}) E(z) I(z) + y_{\rm p}(z) + 1, \quad (29)$$

where $y_{\rm p}(z)$ determines the rate of halo merging.[4] However, it is important only for $z \gtrsim 3$ and therefore we neglect it here (see BPR08). Furthermore, we have

$$I(z) = \int_z^\infty \left(\frac{1+x}{E(x)} \right)^3 {\rm d}x, \quad (30)$$

while the constants $\mathcal{C}_1$ and $\mathcal{C}_2$ have been fitted using a ΛCDM simulation with $\Omega_{\rm m} = 0.3$ and $\sigma_8 = 0.9$ (BPR08), and have been found to follow the form

$$\mathcal{C}_{1,2}(M_{\rm h}) \simeq \alpha_{1,2} \left(\frac{M_{\rm h}}{10^{13}\, h^{-1}\, {\rm M}_\odot} \right)^{\beta_{1,2}}, \quad (31)$$

with $\beta_1 = 0.34$, $\beta_2 = 0.32$, while α_1 and α_2 have been found to be cosmological model dependent, with values given by (Papageorgiou et al., in preparation)

$$\alpha_1 \simeq \kappa_1 \left(\frac{0.9}{\sigma_8} \right)^{\kappa_2} \exp\left[\kappa_3(\Omega_{\rm m} - 0.3)\right], \quad (32)$$

with $\kappa_1 \simeq 3.44$, $\kappa_2 \simeq 2/5$ and $\kappa_3 \simeq 4/5$, and

$$\alpha_2 \simeq -0.36 \left(\frac{\Omega_{\rm m}}{0.3} \right)^{3/2}. \quad (33)$$

(iii) *Non-linear power spectrum*. Since the correlation function on small angular scales is within the expected non-linear regime, we should include in our model power spectrum the non-linear contributions. To this end we use the corresponding fitting formula introduced by Peacock & Dodds (1996) for the ΛCDM model (see also Smith et al. 2003; Widrow et al. 2009). There is one relatively free parameter in their formulation, which is the slope of the power spectrum at the relevant scales, since the CDM power spectrum curves slowly and thus it varies as a function of scale: $n_{\rm eff} = {\rm d ln}\, P(k)/{\rm d ln}\, k$. On the scales of interest the value is $n_{\rm eff} \simeq -2$, but we have decided to actually derive, and then fix, the $n_{\rm eff}$ value from the data analysis itself. Using the minimization procedure discussed in Section 3.3 we compare the observed 2*XMM* AGN correlation function with that provided by the *WMAP*7 ΛCDM model (i.e. fixing $\Omega_{\rm m} = 0.272$, $w = -1$ and $\sigma_8 = 0.811$) fitting the remaining two free parameters (i.e. $M_{\rm h}$ and $n_{\rm eff}$). The corresponding solution space can be seen in Fig. 12, while the best-fitting parameter values are $M_{\rm h} \simeq 6.5(\pm 2.1) \times 10^{12}\, h^{-1}\, {\rm M}_\odot$ and $n_{\rm eff} \simeq -2.02^{+0.05}_{-0.04}$. In the

[4] Note that the bias factor at the present time is given by $b(M_{\rm h}, 0) = \mathcal{C}_1(M_{\rm h}) + \mathcal{C}_2(M_{\rm h}) I(0) + 1$.

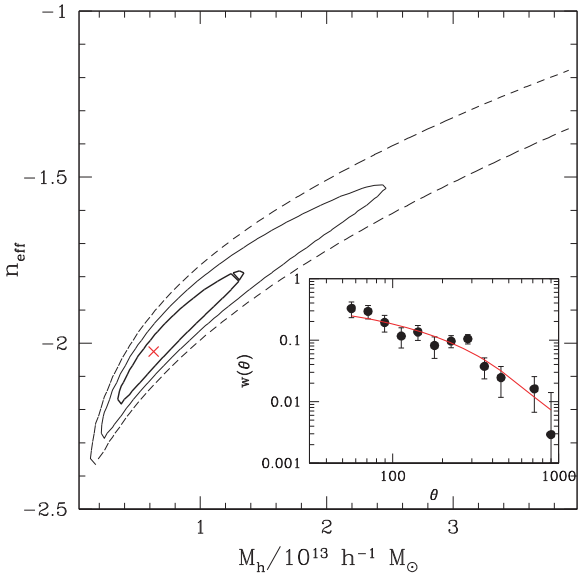

Figure 11. Main panel: the 1, 2 and 3σ likelihood contours in the $M_{\rm h}$, $n_{\rm eff}$ parameter space for the ΛCDM (*WMAP*7) model. Inner panel: the Ebrero et al. (2009b) 2*XMM* angular correlation function and the best-fitting ΛCDM model (continuous line).

inset of Fig. 11 we also plot the 2*XMM* angular correlation function together with the best-fitting ΛCDM model (continuous line).

As a consistency check we have verified that when fixing the non-linear slope of $P(k)$ to the above fitted value and leave as free parameters $M_{\rm h}$ and σ_8, we recover the *WMPA*7 σ_8 value and exactly the same $M_{\rm h}$ value, as above. The derived value of $M_{\rm h}$ is slightly larger than that provided by Ebrero et al. (2009b) using the Sheth et al. (2001) bias evolution model (i.e. $\simeq 5 \times 10^{12}\,h^{-1}\,{\rm M}_{\odot}$). We have tested also the case of a clustering evolution model with $\epsilon = -3$, in which case the derived value of the halo mass is $\simeq 2 \times 10^{10}\,h^{-1}\,{\rm M}_{\odot}$, a value significantly below any reasonable value that has been proposed or derived in the literature. We will therefore use $\epsilon = -1.2$ throughout the rest of the paper.

3.3 Fitting models to the 2*XMM* clustering data

In order to constrain the cosmological parameters we use again the standard χ^2 likelihood procedure and compare the measured *XMM* soft-band source angular correlation function (Ebrero et al. 2009b) with the predictions of different spatially flat cosmological models. The corresponding likelihood estimator is defined as $\mathcal{L}_{\rm AGN}(\boldsymbol{p}) \propto \exp[-\chi^2_{\rm AGN}(\boldsymbol{p})/2]$ with

$$\chi^2_{\rm AGN}(\boldsymbol{p}) = \sum_{i=1}^{n} \frac{[{\rm w_{th}}(\theta_i, \boldsymbol{p}) - {\rm w_{obs}}(\theta_i)]^2}{\sigma_i^2 + \sigma_{\theta_i}^2}, \qquad (34)$$

where $\boldsymbol{p} \equiv (\Omega_{\rm m}, w, M_{\rm h})$, σ_i is the uncertainty of the observed angular correlation function and σ_{θ_i} corresponds to the width of the angular separation bins.

We sample the various parameters as follows: the matter density $\Omega_{\rm m} \in [0.1, 0.4]$ in steps of 0.002; the equation of state parameter $w \in [-1.4, -0.6]$ in steps of 0.005 and the parent DM halo $M_{\rm h}/10^{13}\,h^{-1}\,{\rm M}_{\odot} \in [0.1, 3]$ in steps of 0.01. In this likelihood analysis we use as priors a flat universe, and the previously mentioned values of h, σ_8 and $\Omega_{\rm b}$.

The results of the minimization procedure for the case of $\sigma_8 = 0.81$ are $\Omega_{\rm m} = 0.301 \pm 0.008$, $w = -0.990 \pm 0.058$ and $M_{\rm h} = 3.1(\pm 1.1) \times 10^{12}\,h^{-1}\,{\rm M}_{\odot}$, with a $\chi^2 = 39.41$ for 10 degrees of freedom (dof). The large value of χ^2/dof is due to the sinusoidal modulation of the 2*XMM* w(θ), which could be due to systematic effects possibly related to the size of the *XMM* fields (see discussion in BP09). If we use the 2σ w(θ) uncertainty in the denominator of the χ^2 function of equation (34), then the χ^2 drops to $\simeq$9.86 (and the uncertainties of the fitted parameters increase to roughly twice the values indicated previously).

These results slightly differ with respect to the similar analysis of BP09 due to a number of improvements that we have currently included, apart from the fact that we have also used the *WMAP*7 cosmological parameters (i.e. $\Omega_{\rm b}$, n and h). The two main improvements have to do with (a) the bias evolution model, in which we have now taken into account the dependence of the parameter a_1 (see equation 32) on $\Omega_{\rm m}$ and σ_8 (which has mostly affected the derived value of $M_{\rm h}$, reducing it significantly), and (b) the non-linear power-spectrum corrections, for which we have used the Peacock & Dodds (1996) ΛCDM fitting formula.

Nevertheless, our current procedure can and will be improved in the future in a number of ways.

(i) We will eventually use the clustering of X-ray-selected AGN from a large contiguous X-ray survey, a fact which will solve, we believe, the quasi-sinusoidal small amplitude modulation of the 2*XMM* w(θ) (see discussion in BP09). Such a future survey is the *XMM–Newton* Very Large Programme (XXL), which was recently granted time to map two extragalactic regions of 25 deg^2, at a depth of $\sim 5 \times 10^{-15}$ erg cm^{-2} s^{-1} (Pierre et al. 2011).

(ii) We will investigate more accurate non-linear power-spectrum corrections of w(θ) (e.g. Widrow et al. 2009).

(iii) We will ultimately test a large range of DE equations of state to include CPL and alternative gravity [$f(R)$] models. To this end we will use the recent generalization of the BPR08 bias evolution model of Basilakos, Plionis & Pouri (2011).

4 JOINT HUBBLE RELATION, AGN CLUSTERING AND BAO ANALYSIS

Here we will perform an example of the joint analysis between the previously discussed results from 2*XMM* clustering and the Hubble relation, which is the basic aim of our overall project. For the current exercise we will use the *Constitution* SNIa Hubble relation since we are still working on the development of the H II-galaxy-based methodology. For completeness we will also use the recent results of the BAO technique. We remind the reader that BAOs are produced by pressure (acoustic) waves in the photon–baryon plasma in the early universe generated by DM overdensities. At the recombination era ($z \sim 1100$), photons decouple from baryons and free stream while the pressure wave stalls. Its frozen scale, which constitutes a standard ruler, is equal to the sound horizon length, $r_{\rm s} \sim 100\,h^{-1}$ Mpc (e.g. Eisenstein & Hu 1998). This appears as a small, $\sim$10 per cent excess in the galaxy, cluster or AGN power spectrum (and its Fourier transform, the two-point correlation function) at a scale corresponding to $r_{\rm s}$. First evidence of such an excess have been reported in the clustering of the SDSS LRGs (see Eisenstein et al. 2005; Padmanabhan et al. 2007; Percival et al. 2010). In this work we use the latest measurement of Percival et al. (2010):

$$r_{\rm s}(z_{\rm d})/D_{\rm V}(z_{\star}) = 0.1390 \pm 0.0037$$

(see also Kazin et al. 2010a,b). Note that $r_{\rm s}(z_{\rm d})$ is the comoving sound horizon size at the baryon drag epoch $z_{\rm d}$, which is given by the fitting formula of Eisenstein & Hu (1998), $D_{\rm V}(z_{\star})$ is the effective distance measure and $z_{\star} = 0.275$. Of course, the quantities $r_{\rm s}, D_{\rm V}$

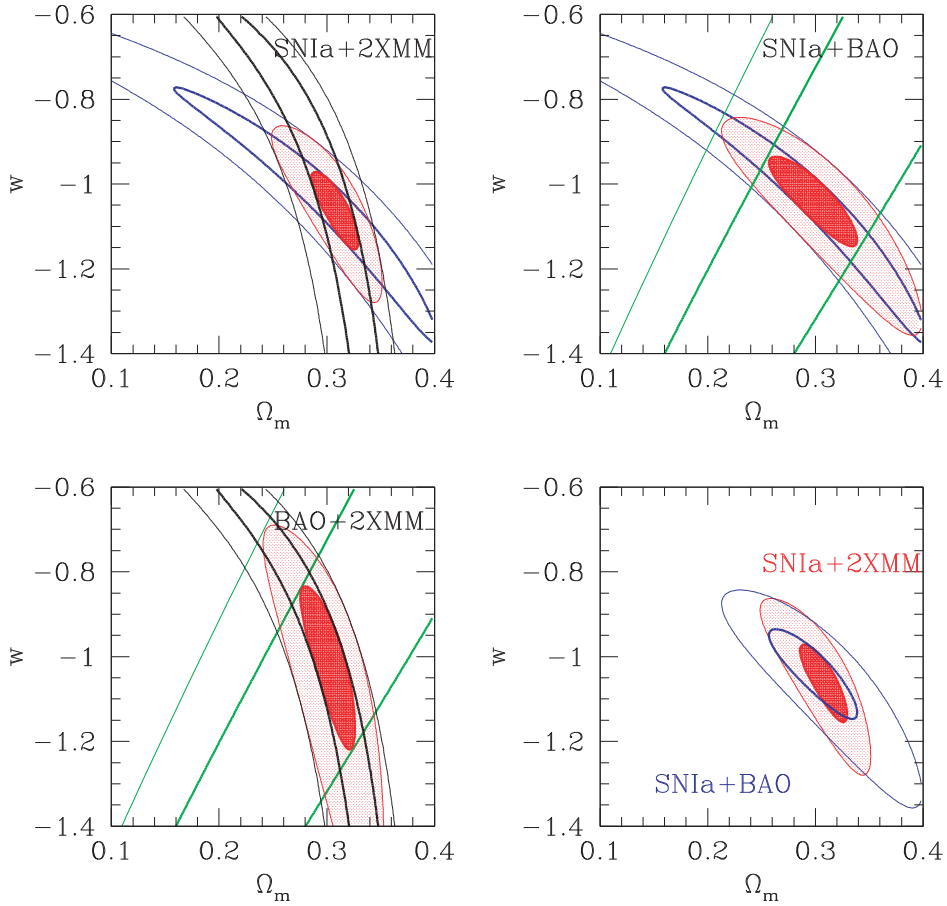

Figure 12. QDE model parameter constraints (i.e. in the Ω_m, w plane) provided by the joint likelihood analysis of pairs of cosmological data. The red shaded contours are the joint likelihood contours of the indicated pairs of data. For clarity we show only contours corresponding to the 1 and 3σ confidence levels. The 2*XMM* results shown correspond to those based on a power spectrum normalization of $\sigma_8 = 0.81$. Note also that we have followed the conservative approach of using 2σ w(θ) uncertainties in the minimization process, to allow for the small amplitude sinusoidal w(θ) modulation (see main text and BP09). Upper left-hand panel: *Constitution* SNIa Hubble relation (blue contours) and 2*XMM* AGN clustering (black contours). Upper right-hand panel: *Constitution* SNIa Hubble relation (blue contours) and LRGs BAO (green contours). Lower left-hand panel: 2*XMM* AGN clustering (black contours) and LRGs BAO (green contours). Lower right-hand panel: the joint likelihood contours of the SNIa–2*XMM* (red contours) and of the SNIa–BAO (blue contours) pairs.

can be defined analytically, and are given by

$$r_s(z_d) = \frac{c}{\sqrt{3}} \int_0^{a_d} \frac{da}{a^2 H(a) \sqrt{1 + (3\Omega_b/4\Omega_\gamma)a}}, \quad (35)$$

where $a_d = (1 + z_d)^{-1}$ and $\Omega_\gamma h^2 \simeq 2.47 \times 10^{-5}$ the energy density of photons. In this context, the effective distance is (Eisenstein et al. 2005)

$$D_V(z) \equiv \left[(1+z)^2 D_A^2(z) \frac{cz}{H(z)} \right]^{1/3}, \quad (36)$$

where $D_A(z)$ is the angular diameter distance. Therefore, the corresponding χ^2_{BAO} function is simply written as

$$\chi^2_{BAO}(\boldsymbol{p}) = \frac{[(r_s(z_d))/(D_V(z_\star))(\boldsymbol{p}) - 0.1390]^2}{0.0037^2}, \quad (37)$$

where $\boldsymbol{p}$ is the vector containing the cosmological parameters that we want to fit for. In this case $\boldsymbol{p} = (\Omega_m, w)$.

We therefore perform a joint likelihood analysis, assuming that any two pairs of cosmological data sets are independent (which indeed they are) and thus the joint likelihood can be written as the product of the two individual ones. The results based on the joint analysis of the different pairs of cosmological data are shown in Fig. 12 and quantified in Table 3. It is evident that the addition of the *XMM* clustering analysis provides significantly more stringent constraints than, for example, the joint SNIa and BAO results. The *reduction parameter*, i.e. the ratio of the FoM of the joint

Table 3. The best-fitting values of the cosmological parameters based on the joint likelihood analysis of the indicated cosmological data. For the case of the 2*XMM* clustering analysis we followed the conservative approach of using 2σ w(θ) uncertainties. The uncertainty of each fitted cosmological parameter has been estimated after marginalizing over the other parameter (i.e. by fixing one parameter at its best value and allowing the other to vary, providing as its uncertainty the range for which $\Delta\chi^2 \leq 2.3$). The last column indicates the *reduction parameter* (related to the FoM) as defined in Section 2.3.4.

Joint data	Ω_m	w	χ^2	dof	S
SNIa+BAO	0.296 ± 0.021	-1.027 ± 0.053	439.711	365	2.32
XMM[a]+SNIa	0.310 ± 0.012	$-1.064 \pm {}^{0.053}_{0.048}$	449.591	374	4.49
XMM[a]+BAO	0.302 ± 0.014	$-0.995 \pm {}^{0.096}_{0.128}$	9.860	11	1.74
XMM[b]+SNIa	0.318 ± 0.013	$-1.085 \pm {}^{0.059}_{0.048}$	449.644	374	4.35
XMM[b]+BAO	0.306 ± 0.015	$-0.973 \pm {}^{0.096}_{0.123}$	9.861	11	1.70

[a]2*XMM* results based on a $P(k)$ normalization of $\sigma_8 = 0.811$.
[b]Based on $\sigma_8 = 0.78$.

XMM–SNIa analysis to that of the *Constitution* SNIa analysis (see definition in Section 2.3.4) shows that the 2σ range of the (Ω_m, w) solution space is reduced by a factor of $\sim$2 with respect to that of the BAO–SNIa analysis (see lower right-hand panel of Fig. 12).

The necessity, however, to impose constraints on a more general, time-evolving, DE equation of state (equation 2), implies that there is ample space for improving the current analysis and indeed our aim is to develop further this project by (a) using a new Hubble relation analysis, based on high-z H II galaxies, as detailed in this paper, and (b) by generalizing the BPR08 bias evolution model for any DE equation of state (CPL and alternative gravity models).

5 CONCLUSION

We have investigated the question of which is the most efficient strategy to tighten the cosmological constraints provided by fitting the Hubble relation. Using extensive Monte Carlo simulations we have verified that by using only a few tens of high-z tracers (in the range $2 \lesssim z \lesssim 3.5$), even with a relatively large distance modulus uncertainty, we can reduce significantly the present cosmological parameter solution space. We have taken into account the effects of lensing magnification/demagnification, which not only increases the distance modulus uncertainty but it also shifts systematically the mean distance modulus of individual sources. Although the effects can be severe for an individual source, they can be statistically treated and they are significantly reduced the denser the source sampling is in redshift space. Applying our lensing magnification correction to the *Constitution* SNIa set (Hicken et al.), we find that the fitted cosmological parameters are not significantly affected by such effects due to the fact that the SNIa sample traces relatively small redshifts ($z \lesssim 1$).

Based on a FoM analysis we have provided a simple procedure to estimate the necessary number of $2 \lesssim z \lesssim 3.5$ tracers needed to reduce the cosmological solution space, presently provided by the *Constitution* set, by a desired factor of our choice and for any level of rms distance modulus uncertainty. This analysis has shown that in order to significantly reduce the cosmological parameter solution space, it is more efficient to increase the number of high-z tracers than to reduce their individual uncertainties. A re-analysis of the cosmological constraints provided by a small sample of high-z ($2.2 \lesssim z \lesssim 3.4$) H II galaxies, previously analysed by Siegel et al. (2005), but now using a novel determination of the zero-point of the relevant distance scaling relation, provides consistent cosmological results with those of SNIa, although the DE equation of state parameter remains unconstrained at present.

Finally, using the clustering of X-ray-selected AGN we provide the framework that will be used, joining their cosmological likelihood with that of the Hubble relation analysis, to put stringent DE equation of state constraints. An example of such a joint analysis, using the 2*XMM* clustering and the *Constitution* SNIa Hubble relation, and under the priors of a flat universe, $h = 0.704$ and $\sigma_8 = 0.81$ or 0.78, provides significantly more stringent QDE model constraints, as indicated by the fact that the FoM increases by a factor of $\sim$2, with respect to that of the joint SNIa–BAO analysis. The QDE cosmological parameters provided by the 2*XMM*–SNIa joint analysis are $\Omega_m = 0.31 \pm 0.01$ and $w = -1.06 \pm 0.05$, with the uncertainties being estimated after marginalizing one parameter over the other.

ACKNOWLEDGMENTS

We thank Dr J. Ebrero for comments and for providing us with an electronic version of the clustering results and their *XMM* survey area curve. MP, RT and ET also acknowledge financial support under Mexican government CONACyT grants 2005-49878, 2005-49847 and 2007-84746 and 2008-103365, respectively.

REFERENCES

Adak D., Bandyopadhyay A., Majumdar D., 2011, preprint (arXiv:1102.4726)
Akylas A., Georgantopoulos I., Plionis M., 2000, MNRAS, 318, 1036
Albrecht A. et al., 2006, preprint (astro-ph/0609591)
Allen S. W., Schmidt R. W., Ebeling H., Fabian A. C., van Speybroeck L., 2004, MNRAS, 353, 457
Amanullah R. et al., 2010, ApJ, 716, 712
Astier P. et al., 2006, A&A, 447, 31
Atek H. et al., 2010, ApJ, 723, 104
Bardeen J. M., Bond J. R., Kaiser N., Szalay A. S., 1986, ApJ, 304, 15
Barlow R., 2004, preprint (arXiv:physics/0406120)
Basilakos S., Perivolaropoulos L., 2008, MNRAS, 391, 411
Basilakos S., Plionis M., 2001, ApJ, 550, 522
Basilakos S., Plionis M., 2003, ApJ, 593, L61
Basilakos S., Plionis M., 2005, MNRAS, 360, L35
Basilakos S., Plionis M., 2006, ApJ, 650, L1
Basilakos S., Plionis M., 2009, MNRAS, 400, L57 (BP09)
Basilakos S., Plionis M., 2010, ApJ, 714, L185
Basilakos S., Georgakakis A., Plionis M., Georgantopoulos I., 2004, ApJ, 607, L79
Basilakos S., Plionis M., Georgantopoulos I., Georgakakis A., 2005, MNRAS, 356, 183
Basilakos S., Plionis M., Ragone-Figueroa C., 2008, ApJ, 678, 627 (BPR08)
Basilakos S., Plionis M., Pouri A., 2011, Phys. Rev. D, 83, 123525
Bassett B. A., 2005, Phys. Rev. D, 71, 083517
Blake C., Collister A., Bridle S., Lahav O., 2007, MNRAS, 374, 1527
Boyle B. J., Mo H. J., 1993, MNRAS, 260, 925
Brouzakis N., Tetradis N., 2008, Phys. Lett. B, 665, 344
Bueno Sanchez J. C., Nesseris S., Perivolaropoulos L., 2009, J. Cosmol. Astropart. Phys., 11, 029
Cappelluti N., Ajello M., Burlon D., Krumpe M., Miyaji T., Bonoli S., Greiner J., 2010, ApJ, 716, L209
Carrera F. J., Barcons X., Fabian A. C., Hasinger G., Mason K. O., McMahon R. G., Mittaz J. P. D., Page M. J., 1998, MNRAS, 299, 229
Carrera F. J. et al., 2007, A&A, 469, 27
Chevallier M., Polarski D., 2001, Int. J. Modern Phys. D, 10, 213
Coil A. et al., 2009, ApJ, 701, 1484
Davis T. M. et al., 2007, ApJ, 666, 716 (D07)
de Zotti G., Persic M., Franceschini A., Danese L., Palumbo G. G. C., Boldt E. A., Marshall F. E., 1990, ApJ, 351, 22
Dicus D. A., Repko W. W., 2004, Phys. Rev. D, 70, 3527
Ebrero J. et al., 2009a, A&A, 493, 55
Ebrero J., Mateos S., Stewart G. C., Carrera F. J., Watson M. G., 2009b, A&A, 500, 749
Eisenstein D. J., Hu W., 1998, ApJ, 496, 605
Eisenstein D. J. et al., 2005, ApJ, 633, 560
Erb D. K. et al., 2003, ApJ, 591, 101
Erb D. K., Steidel C. C., Shapley A. E., Pettini M., Reddy N. A., Adelberger K. L., 2006a, ApJ, 646, 107
Erb D. K., Steidel C. C., Shapley A. E., Pettini M., Reddy N. A., Adelberger K. L., 2006b, ApJ, 647, 128
Freedman W. L. et al., 2001, ApJ, 553, 47
Gandhi P. et al., 2006, A&A, 457, 393
Ghirlanda G., 2009, preprint (arXiv:0908.1930)
Ghirlanda G., Ghisellini G., Firmani C., 2006, New J. Phys., 8, 123
Gilli R. et al., 2005, A&A, 430, 811
Hicken M. et al., 2009, ApJ, 700, 1097
Holz E. D., Linder E. V., 2005, ApJ, 631, 678 (HL05)
Holz E. D., Wald R. M., 1998, Phys. Rev. D, 58, 063501
Hudson M. J., Smith R. J., Lucey J. R., Schlegel D. J., Davies R. L., 1999, ApJ, 512, L79

Kazaku Y., Cowie L. L., Hu E. M., 2007, ApJ, 668, 853
Kazin E. A. et al., 2010a, ApJ, 710, 1444
Kazin E. A., Blanton M. R., Scoccimarro R., McBride C. K., Berlind A. A., 2010b, ApJ, 719, 1032
Kim A. G., 2011, PASP, 123, 230
Komatsu E. et al., 2009, ApJS, 180, 330
Komatsu E. et al., 2011, ApJS, 192, 18
Koo D. C. et al., 1996, ApJ, 469, 535
Kowalski M. et al., 2008, ApJ, 686, 749
Krumpe M., Miyaji T., Coil A. L., 2010, ApJ, 713, 558
Kundić T., 1997, ApJ, 482, 631
Li X.-D., Li S., Wang S., Zhang W.-S., Huang Q.-G., Li M., 2011, J. Cosmol. Astropart. Phys., 07, 011
Limber D. N., 1953, ApJ, 117, 134
Linder V. E., 2003, Phys. Rev. Lett., 90, 091301
Ma C.-P., Maggiore M., Riotto A., Zhang J., 2011, MNRAS, 411, 2644
Manners J. C. et al., 2003, MNRAS, 343, 293
March M. C., Trotta R., Berkes P., Starkman G. D., Vaudrevange P. M., 2011, preprint (arXiv:1102.3237)
Matarrese S., Coles P., Lucchin F., Moscardini L., 1997, MNRAS, 286, 115
Mateos S. et al., 2008, A&A, 429, 51
Matsubara T., 2004, ApJ, 615, 573
Melnick J., 1978, A&A, 70, 157
Melnick J., 2003, in Perez E. et al., eds, ASP Conf. Ser. Vol. 297, Star Formation Through Time. Astron. Soc. Pac., San Francisco, p. 3
Melnick J., Moles M., Terlevich R., Garcia P., Jose M., 1987, MNRAS, 226, 849
Melnick J., Terlevich R., Moles M., 1988, MNRAS, 235, 313
Melnick J., Terlevich R., Terlevich E., 2000, MNRAS, 311, 629
Miyaji T. et al., 2007, ApJS, 172, 396
Mo H. J., White S. D. M., 1996, MNRAS, 282, 347
Mullis C. R., Henry J. P., Gioia I. M., Böhringer H., Briel U. G., Voges W., Huchra J. P., 2004, ApJ, 617, 192
Nestor D. B., Shapley A. E., Steidel C. C., Siana B., 2011, ApJ, 736, 18
Padmanabhan N. et al., 2007, MNRAS, 378, 852
Peacock J. A., Dodds S. J., 1996, MNRAS, 280, L19
Peacock J. A. et al., 2006, preprint (astro-ph/0610906)
Peebles P. J. E., Ratra B., 2003, Rev. Modern Phys., 75, 559
Percival W. J. et al., 2010, MNRAS, 401, 2148
Perlmutter S. et al., 1998, Nat, 391, 51
Perlmutter S. et al., 1999, ApJ, 517, 565
Pettini M. et al., 2001, ApJ, 554, 981
Pierre M., Pacaud F., Juin J. B., Melin J. B., Clerc N., Corasaniti P. S., 2011, MNRAS, 414, 1732
Plionis M., Rovilos M., Basilakos S., Georgantopoulos I., Bauer F., 2008, ApJ, 674, L5
Plionis M., Terlevich R., Basilakos S., Bresolin F., Terlevich E., Melnick J., Georgantopoulos I., 2009, J. Phys. Conf. Ser., 189, 012032
Puccetti S. et al., 2006, A&A, 457, 501
Riess A. G. et al., 1998, AJ, 116, 1009
Riess A. G. et al., 2004, ApJ, 607, 665
Riess A. G. et al., 2007, ApJ, 659, 98
Sánchez A. G., Crocce M., Cabré A., Baugh C. M., Gaztañaga E., 2009, MNRAS, 400, 1643
Schuecker P., Caldwell R. R., Böhringer H., Collins C. A., Guzzo L., Weinberg N. N., 2003, A&A, 402, 53
Seljak U. et al., 2005, Phys. Rev. D, 71, 3515
Sheth R. K., Tormen G., 1999, MNRAS, 308, 119
Sheth R. K., Mo H. J., Tormen G., 2001, MNRAS, 323, 1
Siegel E. R., Guzmán R., Gallego J. P., Orduña López M., Rodríguez Hidalgo P., 2005, MNRAS, 356, 1117
Smith R. E. et al., 2003, MNRAS, 341, 1311
Spergel D. N. et al., 2003, ApJS, 148, 175
Spergel D. N. et al., 2007, ApJS, 170, 377
Starikova S. et al., 2010, preprint (arXiv:1010.1577)
Straughn A. et al., 2011, AJ, 141, 14
Sugiyama N., 1995, ApJS, 100, 281
Tegmark M. et al., 2004, Phys. Rev. D, 69, 3501
Terlevich R., Melnick J., 1981, MNRAS, 195, 839
Tinker J. L., Robertson B. E., Kravtsov A. V., Klypin A., Warren M. S., Yepes G., Gottlöber S., 2010, ApJ, 724, 878
Tonry J. et al., 2003, ApJ, 594, 1
Vikhlinin A., Forman W., 1995, ApJ, 455, 109
Wang Y., Mukherjee P., 2006, ApJ, 650, 1
Wang Y., Holz D. E., Munshi D., 2002, ApJ, 572, L15
Wang S., Li X.-D., Li M., 2011, Phys. Rev. D, 83, 3010
Wei H., 2008, European Phys. J. C, 60, 449
Widrow L. M., Elahi P. J., Thacker R. J., Richardson M., Scannapieco E., 2009, MNRAS, 397, 1275
Wood-Vasey W. M. et al., 2007, ApJ, 666, 694
Xia L. et al., 2011, AJ, 141, 64
Yamada S. et al., 2005, PASJ, 57, 881
Yang Y., Mushotzky R. F., Barger A. J., Cowie L. L., Sanders D. B., Steffen A. T., 2003, ApJ, 585, L85
Yang Y., Mushotzky R. F., Barger A. J., Cowie L. L., 2006, ApJ, 645, 68

This paper has been typeset from a TEX/LATEX file prepared by the author.